TAMPEREEN TEKNILLINEN YLIOPISTO
TAMPERE UNIVERSITY OF TECHNOLOGY

ARASH NASSAJY

OPTIMIZATION OF ORGANIC SCHOTTKY DIODE CONTACT BY ELECTROCHEMICAL TREATMENT OF ELECTRODES

Master of Science Thesis

Examiner: Professor Donald Lupo
Examiner and topic approved by the
Council of the Faculty of Computing
and Electrical Engineering on
May 2015

ABSTRACT

TAMPERE UNIVERSITY OF TECHNOLOGY
Master's Degree Programme in Electrical Engineering
NASSAJY, ARASH: Optimization of Organic Schottky Diode Contact by Electrochemical Treatment of Electrodes
Master of Science Thesis, 51 pages
May 2015
Major: Radio Frequency Electronics
Examiner(s): Professor Donald Lupo
Keywords: anodization, energy harvesting, organic printed electronics, rectifier, RFID, Schottky diode

The development of the organic printed electronics facilitates manufacturing low-cost, light-weighted flexible electronic components and circuits. The flexible circuits have the potential to be widely used in the future electronic systems. For instance, the chip used in the passive Radio Frequency Identification (RFID) tags can be fabricated on flexible substrates. These passive tags acquire their energy from the incident electromagnetic waves via a harvesting circuit.

The Schottky diode is the main part of the harvesting circuit in order to rectify the input AC signal and deliver the DC output signal required to power the main circuit. The acquired energy is augmented if the rectification ratio of the diode increases. The rectification ratio increases through increasing the forward current or reducing the reverse current of the diode, which can be realized by optimizing the metal-semiconductor interfaces. In fact, the optimization of the ohmic contact increases the forward current, whereas optimizating the Schottky contact decreases the reverse current of the diode.

In this thesis, the optimization of the ohmic silver-semiconductor interface of the organic Schottky diode has been studied. The optimization is fulfilled through controlling the thickness of the silver oxide layer by utilizing anodization as an electrochemical treatment. The performance of the diode was evaluated by examining the current-voltage and AC rectification characteristics of the diode. It was observed that the forward current, and accordingly, the rectification ratio of the diode increases as the thickness of the anodic oxide layer increases. The augment of the rectification ratio increases the DC output voltage of the half-wave rectifying circuit. However, the existence of the charged traps influences the DC outputs of the rectifier for the diodes with the same rectification ratios.

PREFACE

This master thesis was done in the Organic Electronics Group (OEG) in the Department of Electronics and Communications Engineering at Tampere University of Technology (TUT) in partial fulfilment of the requirements for the Master of Science degree in Radio Frequency Electronics. The research was funded and supported by the Academy of Finland.

I would like to thank my thesis examiner Prof. Donald Lupo for all his invaluable supports and guidance throughout the work. I really appreciate him having provided me with the opportunity to complete my thesis under his supervision. I am also thankful to all my colleagues in the OEG for their help and support. I am really grateful that my thesis was accomplished in such a convivial atmosphere.

Finally, I tip my hat to my parents to express my deepest gratitude and love for all their gentleness and thoughtfulness.

Tampere, May 2015

ARASH NASSAJY

TABLE OF CONTENTS

LIST OF FIGURES

LIST OF TABLES

LIST OF ABBREVIATIONS AND SYMBOLS

AC	Alternative current
CE	Counter electrode
DC	Direct current
DI	Distilled
ECE	Electrochemical equivalent
HF	High frequency
HOMO	Highest occupied molecular orbital
IPA	Isopropyl alcohol
ISO	International Organization for Standardization
LCAO	Linear combination of atomic orbitals
LUMU	Lowest unoccupied molecular orbital
MIM	Metal-insulator-metal
MS	Metal-semiconductor
OLED	Organic light-emitting diode
OTFT	Organic thin film transistor
PEDOT:PSS	Poly(3,4-ethylenedioxythiophene):poly(styrenesulfonate)
PEEk	Polyether ether ketone
PET	Poly(ethylene terephthalate)
PEN	poly(ethylene naphthalate)
PTAA	Poly(triarylamine)
R2R	Roll-to-roll or reel-to-reel
RE	Reference electrode
RF	Radio frequency
RFID	Radio frequency identification
SCLC	Space charge limited current
UV	Ultraviolet
WE	Working electrode

A	Area
C	Capacitance
C_L	Load capacitance
d_{ox}	Anodized oxide thickness
e	Electrochemical equivalent
E	Chemical equivalent weight
E_C	Semiconductor conduction band edge
E_F	Fermi level
$E_{F,M}$	Metal Fermi level
$E_{F,SC}$	Semiconductor Fermi level

E_g	Band gap energy level
E_V	Semiconductor valence band edge
E_{VAC}	Vacuum energy level
f_{max}	Maximum operation frequency
I_0	Reverse saturation current
J	Current density
J_{diff}	Diffusion current density
J_{drift}	Drift current density
k	Boltzmann constant
L	Thickness of the semiconductor layer
M	Molar mass
M_{ox}	Molar mass of the oxide
N_A	Density of dopants
N_v	Charge-carrier density at the ohmic contact interface
p	Gas pressure
q, Q	Elementary charge
$q\Phi$	Work function
$q\Phi_B$	Schottky barrier energy level
$q\Phi_M$	Metal work function
$q\Phi_S$	Semiconductor work function
$q\chi$	Semiconductor electron affinity
r	Effective molecular radius
R_L	Load resistance
T	Temperature
T_g	Transition temperature
t_T	Transit time
V_0	Contact potential
V_d	Diffusion potential
V_{DC}	Output DC voltage
V_{IN}	Incoming AC signal
V_r	Reverse-biasing voltage
W	Depletion width
ϵ_0	Vacuum permittivity
ϵ_r	Relative permittivity
λ	Mean free path
μ	Semiconductor mobility
ρ_{ox}	Volume density of the oxide
σ	Conductivity

1. INTRODUCTION

The development of the organic semiconductors provides the emergence of the organic electronics. The organic electronics features the capability of printing electronic components on flexible substrates in ambient conditions utilizing the high-throughput roll-to-roll solution processing techniques. Hence, it facilitates the fabrication of cost-effective, lightweight electronic components. Moreover, the organic electronics can manage to deal with one of the big challenges that current industry is encountering, which is environmental friendliness in order to reduce the ambient contamination and global warming.

The organic printed electronics necessitates developing new fabrication steps, and designing novel architectures of the conventional electronic devices. In other words, the structures of the electronic components, like diodes and transistors, need to change so that they can be easily fabricated and printed through a roll-to-roll processing technique. This fact leads to vertically-designed electronic components such as organic thin film transistors (OTFTs), organic light emitting diodes (OLEDs) and solar cells instead of the lateral structures which are common in current electronic industry. In vertical structures, the electronic devices compose of layers, and each layer is printed consecutively. Thus, the surface properties of each layer, on which the next layer is printed, can significantly influence the performance of the device. Moreover, particular interfacial layers can be added to improve the performance of the electronic components.

In this thesis, the metal surface at the ohmic metal-semiconductor interface of an organic Schottky diode is treated in order to optimize the performance of the diode. The optimization treatment is performed using anodization technique. The anodization technique is an electrochemical method to enhance the surface properties of the metals via changing the structure of the metal oxide. Using this technique, it is possible to give stable and uniform colors to the metals. Here, this method is used to control the oxide thickness on top of the metal at metal-semiconductor interface. The effect of the anodic oxide thickness on the performance of the organic Schottky diode is investigated.

In chapter 2, the physics of the organic semiconductors along with the charge carries of this type of semiconductors are discussed. The fabrication techniques used for the organic metal-semiconductor (MS) diodes of this work is reviewed in chapter 3. Also, the physics of the organic MS diodes along with a circuit model to characterize the current-voltage curves are presented in this chapter. The main application of the organic MS or Schottky diodes is in the rectifying circuits to power the RFID tags. The simplest rectifier, that is half-wave rectifier, is used in this work. The fabrication process of the organic Schottky

diodes along with the anodization procedure are presented in chapter 4. In addition, the performance of the diodes is evaluated based on the model presented in chapter 3. Chapter 4 presents the conclusion remarks.

2. THE PHYSICS OF ORGANIC SEMICONDUCTORS

Researching in the field of organic electronic devices requires essential knowledge of the electrical behavior of the organic semiconductors. The transport of charge through an organic semiconductor depends not only on the nature of the molecular conjugation but also on the distortions of the molecular architecture. This chapter presents a rudimentary introduction to the chemical physics of the organic semiconductors, which forms the basis for understanding the electronic properties of the organic electronic devices.

2.1 Organic semiconductor materials

Organic semiconductors are a group of organic materials with semiconductive properties, having electrical conductivities intermediate between insulators and metals. The conductivity of these materials varies over orders of magnitude by changes in temperature, optical excitation and impurity content [1]. This variability of electrical properties induces investigations into the possibility of substituting the current solid state electronic devices with the more futuristic organic printable electronic devices.

Organic semiconductor materials can be found amongst single molecules, oligomers, and organic polymers. The semiconducting polymers are widely utilized in organic printable electronics compared to the other organic semiconductive materials. The reason is the significant difference between the processing of the semiconducting polymers and single-molecule organic semiconductors. In fact, thin films of soluble semicnduvtive polymers can be prepared by solution processing methods, while semicnduvtive molecules are quite often insoluble [2].

Polymers, also known as macromolecules, are composed of a large number of molecular units, known as monomeric units, linked together by covalent bonds. The repeat number of the monomeric unit, denoted by the symbol n, determines the degree of polymerization. Macromolecules are generally obtained by a polymerization process starting from reactive low molar mass compounds [3]. These organic compounds usually contain carbon atoms together with hydrogen, oxygen, nitrogen, and halogen. For instance, the molecular structures of polyethylene and polyacetylene are depicted in Figure 2.1a and 2.1b, respectively. Here, the process is based on ethylene for polyethylene and on acetylene for polyacetylene.

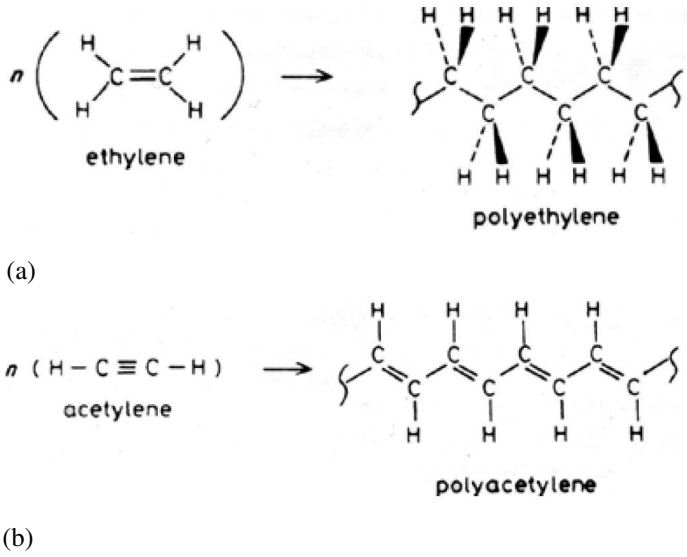

Figure 2.1 *(a) Ethylene and polyethylene, (b) acetylene and polyacetylene*

Polyethylene, like most of the polymers, demonstrates electrically neutral behaviour as insulators do, thus proposes no mobile charges. Furthermore, it possesses no color, and the lowest electronic excitations are in the UV (ultraviolet) region [3]. On the other hand, polyacetylene belongs to a peculiar class of polymers with quite different properties: conjugated polymers. As the name and Figure 2.1 depict, it has conjugated double bonds in the main chain, which makes this kind of polymer behave as semiconductor or conductor and interact with light.

2.1.1 Conjugated polymers

Conjugated polymers are organic macromolecules which are characterized by a backbone chain of alternating double- and single-bonds. Due to the fact that their overlapping p-orbitals create a system of delocalised π-electrons, known as conjugated π-electrons, conjugated polymers behave as one-dimensional semiconductors. The conjugated π-electrons do not belong to one valence band, and their excitation energies are usually in the visible range, thus leading to optically active conjugated polymers [3]. The conductivity and the mechanism of the charge transport in conjugated polymers are explored in section 2.2.

Charges on the backbone chain of a conjugated polymer can also be created by controlled addition of impurities, called doping processes. It means that the organic semiconductors can be doped like the inorganic semiconductors. For example, doping can change polyacetylene from a poor conductor to a good conductor of electric current.

In 1977, Alan J. Heeger, Alan MacDiarmid and Hideki Shirakawa reported high conductivity in oxidized and iodine-doped polyacetylene [4]. They found that the conductivity of thin films of polyacetylene increased tremendously when they were exposed to

iodine vapours. This variability of the conductivity ranges from a basic value at the lower end of the semiconducting range up to the values comparable to metals [4]. Figure 2.2 represents the conductivity changes of polyacetylene in a comparison with other materials. These changes encompass the enormous range of seventeen orders of magnitude. For this research, the 2000 Nobel Prize in Chemistry was awarded to these scientists *"for the discovery and development of conductive polymers."* [5].

Polyacetylene, as the first and the simplest conjugated polymer, did not find practical applications due to the instability in air and the difficulty of preparing films from it [3]. However, this eccentric discovery drew the attention of scientists and triggered intense activities in research and development. Suitable chemical modifications then succeeded to rediscover and produce stable materials, which can be processed from solution or even melt [3]. This easy fabrication along with the mechanical flexibility and low cost give organic semiconductors advantages over inorganic counterparts.

In principle, all devices that can be constructed from the inorganic semiconductors, like diodes and transistors, can also be fabricated from the conjugated polymers. In fact, the organic semiconductors are utilized now as the active elements in optoelectronic devices such as OLED [6], organic solar cells [7], organic field-effect transistors (OFET) [8, 9], electrochemical transistors [10] and recently in biosensing applications [11, 12].

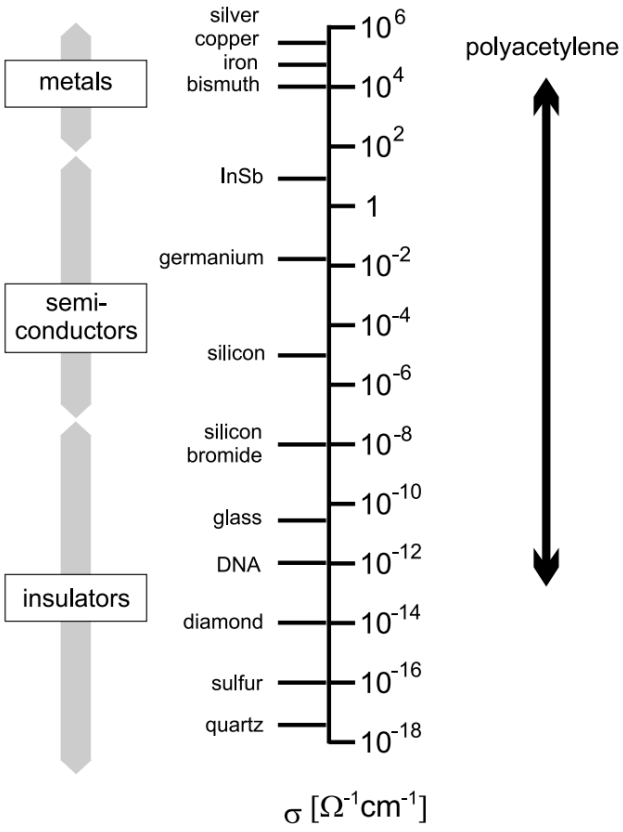

Figure 2.2 *Range of conductivities covered by doped polyacetylene in a comparison with other materials [3].*

2.2 Energy bands and charge transport in conjugated polymers

The specific mechanisms by which current flow in a linear π-conjugated polymer are discussed in this section. Same mechanism applies for cyclic π-conjugated polymers, which are omitted from further discussion for convenience. In examining these mechanisms, it necessitates answering the question of why some organic polymers are good conductors of electric current, whereas others are poor conductors. These fundamental concepts of charge transport form the basis for later discussions of organic electronic devices.

2.2.1 Chemical bonding in organic molecules

In order to understand the chemical bonding in molecules, it is helpful to review the modern atomic model. The modern atomic model comes from the Schrödinger wave equation and quantum mechanics. The Schrödinger equation describes accurately the interactions of particles with potential fields, such as electrons within atoms. By solving this equation, a model for the atom can be obtained. However, only the hydrogen atom is generally solved directly [1]. The hydrogen atom solution is important in identifying the basic selection rules for describing allowed electron energy levels. Namely, electrons are restricted to sets of discrete energy levels within atoms based on this model. Large gaps exist in the energy scale in which no electron energy states are available. It is important to note that only two electrons with opposite spin can occupy each energy state according to the *Pauli exclusion principle*.

Each allowed energy state of the electron in the hydrogen atom is uniquely described by quantum numbers obtained from the solution, and the atomic orbitals are characterized by a unique set of these numbers. The atomic orbitals show the probability of finding an electron around the atom's nucleus, and are the basic building blocks of the atomic orbital model. The first four atomic orbitals are s, p, d and f, respectively. These orbital names are used to describe the electron configurations of the atoms. For instance, electronic configuration of carbon in the ground state is $1s^2\ 2s^2\ 2p^2$, which has two core electrons in shell $n = 1$, and four valence electrons in the $2s$ and $2p$ subshells.

On the valence shell, carbon has two $2s$ and $2p$ electrons. The $2s$ orbital is spherically symmetric with no angular dependency, and is positive everywhere. It can hold two electrons with opposite spin according to the Pauli principle. The $2p$ subshell consists of three orbitals: $2p_{\mathrm{x}}$, $2p_{\mathrm{y}}$ and $2p_{\mathrm{z}}$, which are mutually perpendicular and shaped like dumbbells with a positive lobe and a negative lobe. The $2p$ subshell hold up to six electrons, but only two in the case of carbon. Then, The carbon in the ground state can be read more precisely as $1s^2\ 2s^2\ 2p_x{}^1\ 2p_y{}^1$. When individual carbon atoms are brought very close together, as in the case of C-C backbone of polymers, the s- and p-orbitals overlap so much that they lose their distinct character, and lead to hybridized orbitals. The negative part of the p

orbital cancels the *s*-type orbital, while the positive part enhances it, thereby leading to a directed bond in space. Figure 2.3 illustrates three different kinds of orbital hybridization possible for the pairing electrons in the atomic carbon to form different chemical bonds.

As shown in Figure 2.3, these hybridized orbitals point symmetrically in space, and are responsible for the different molecular geometries. In fact, a tetrahedrally coordinated carbon, as the carbon in methan (CH_4), should possess four orbitals with the correct symmetry to bond to the four hydrogen atoms. This can be done by an excitation of the electron from the doubly occupied $2s$ orbital to the empty $2p_z$ orbital. Hence, the atomic configuration of carbon would change to $1s^2\ 2s^1\ 2p_x{}^1\ 2p_y{}^1\ 2p_z{}^1$, which is suitable for chemical bonding with four hydrogen atoms. Quantum mechanically, the lowest energy is obtained with four equivalent bonds formed from equivalent orbitals on the carbon. This leads to *s*- and *p*-orbitals hybridization to form four sp^3 orbitals point symmetrically in space along the four tetragonal directions (Figure 2.3a). The molecular geometry of the other carbon-based compounds, such as ethylene (C_2H_4) and acetylene (C_2H_2), can be explained in a similar way as methane. In ethylene, the $2s$ orbital mixes with merely two of the three available $2p$ orbitals leading to three hybridized sp^2 orbitals point trigonally symmetrical in space. For acetylene, two of the three $2p$ orbitals remain unchanged, and only one of them blends with $2s$ orbital to make two *sp* orbitals pointing diagonally symmetrical in space. Figure 2.3b and 2.3c depicts the sp^2 and *sp* hybridization, respectively.

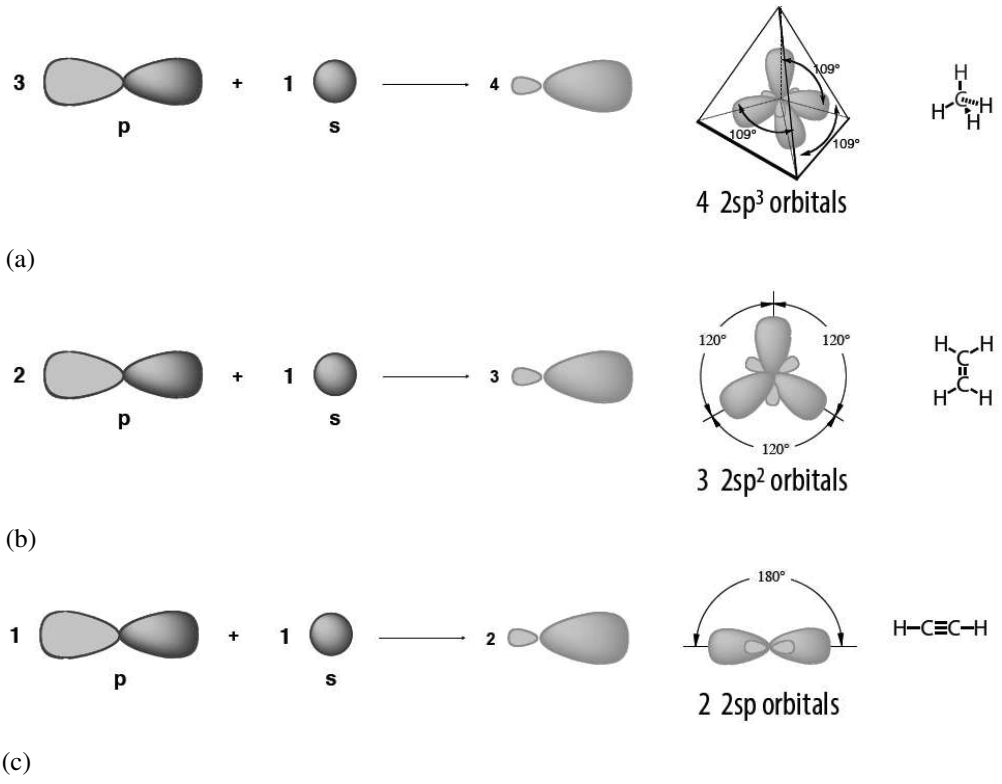

Figure 2.3 *Carbon orbital (a) sp^3, (b) sp^2 and (c) sp hybridizations [13].*

Figure 2.4 shows the chemical bondings for ethane, ethylene and acetylene based on the hybridized carbon atoms. In ethane, the two carbon atoms form a σ bond by overlapping two sp^3 orbitals of each atom (Figure 2.4a). The σ or single bond is the strongest type of covalent bonds with rotational symmetry about the bond axis. In addition to one σ bond, π bonds form between carbon atoms in ethylene and acetylene as shown in Figure 2.4b and 2.4c, respectively. The π bond is usually weaker than σ bond, and forms where two lobes of the residual $2p$ orbital of one atom overlap two lobes of the other parallel residual $2p$ orbital of the contiguous atom. Thus, σ bond have no rotational symmetry around the bond axis. The ethylene molecule has one π bond plus one σ bond leading to a double bond between the carbon atoms, whereas the acetylene possesses two additional π bonds forming triple bond within the molecule. The electrons in π and σ bonds are sometimes referred to as π and σ electrons, respectively.

As isolated carbon atoms are brought together to form a molecule, various interactions occur between neighboring atoms, including previously described orbital hybridizations. Also, important changes occur in the energy level configurations for the electron pairs of the molecular orbitals. The composite two-electron molecular orbitals are linear combinations of the atomic orbitals (LCAO). The odd or antisymmetric combination is called the antibonding orbital, while the even or symmetric combination is the bonding orbital. The σ and π bonds corresponds to the bonding orbitals, whereas the antibonding counterparts are defined as σ^* and π^* orbitals. Figure 2.5 shows the higher energy antibonding and the lower energy bonding orbitals. The highest occupied molecular orbital, here the π orbital, and the lowest unoccupied molecular orbital, here the σ orbital, are abbreviated to HOMO and LUMO, respectively.

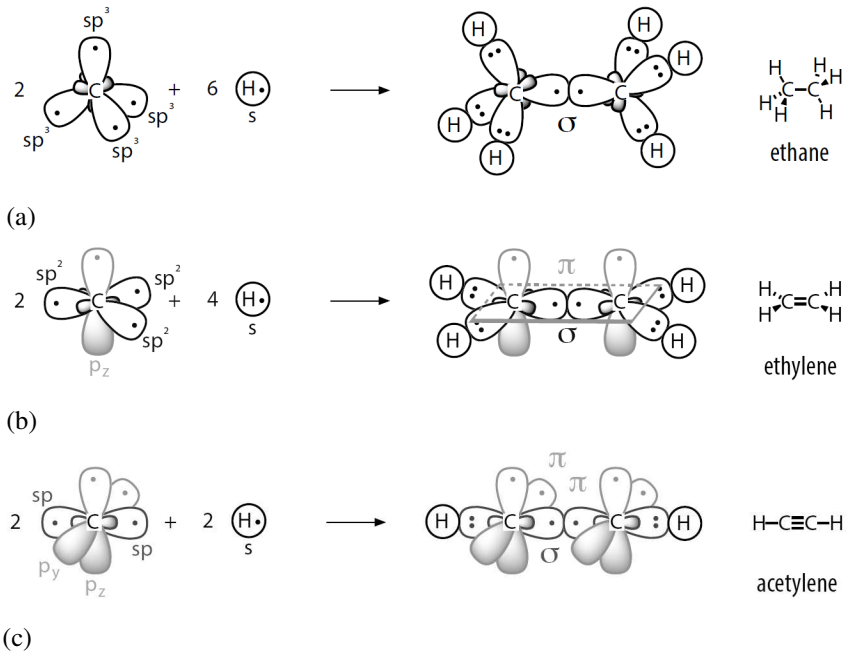

Figure 2.4 *The σ and π bonds for (a) ethan, (b) ethylene and (c) acetylene [13].*

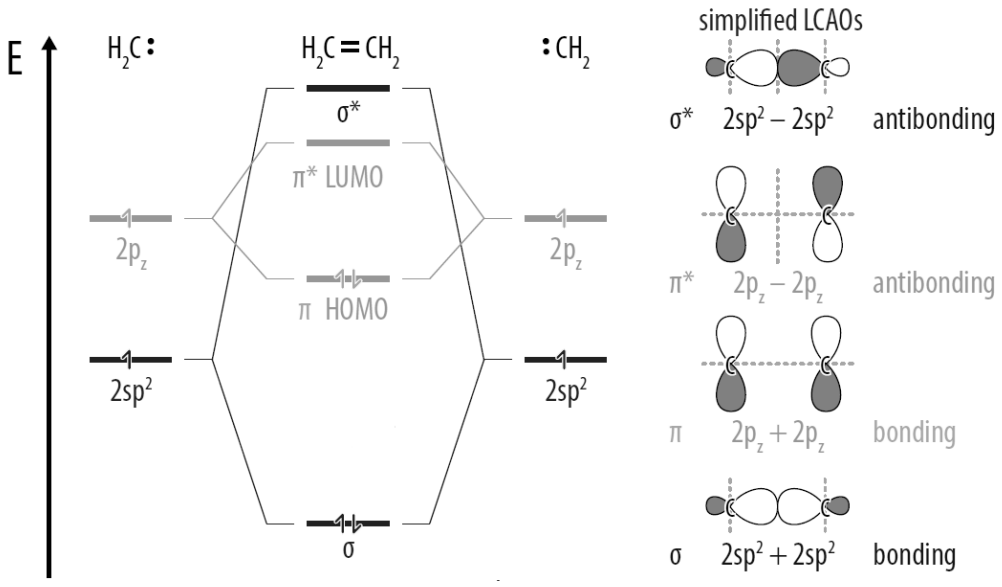

Figure 2.5 *The antibonding and bonding orbitals along with the electron energy level configuration for the ethylene [13].*

2.2.2 Energy bands in conjugated polymers

In a similar fashion, electrons in conjugated polymers are restricted to certain energies and are not allowed in other energies. The basic difference between the case of an electron in a conjugated polymer and that of an electron in a monomer, like ethylene in Figure 2.5, is that the electron has a range, or band, of available energies in the conjugated polymer. In fact, the discrete energy levels of the monomer spread into two bands of energies in the conjugated polymer separated by an *energy gap*, which contains no allowed energy levels for electrons to occupy. The upper band is called the *conduction band*, and the lower one is named the *valence band*. Once the electrons free from the valence band to the conduction band, they are not necessarily localized at a particular carbon atom. Instead, they are *delocalized* and move freely within the molecule. In this situation, the double bonds are delocalized along the polymer chain.

However, the polyacetylene would be a metallic conductor with this model if the distance between all carbon atoms were identical. Actually, the delocalized π-electrons along the main chain of the polyacetylene results in a metal-like, half-filled band with no energy gap. Nonetheless, such an equidistant linear chain metallic structure cannot be stable according to *Pierels' theorem*. In fact, the molecular geometry of the polyacetylene will undergo a structural distortion, called *Pierels transition*, leading to a deformation of alternating shorter double and longer single bonds. This bond length alternation results in a finite band gap for polyacetylene, as shown in Figure 2.6. Figure 2.7 illustrates the imaginary formation of the energy bands and the band gap in the polyacetylene.

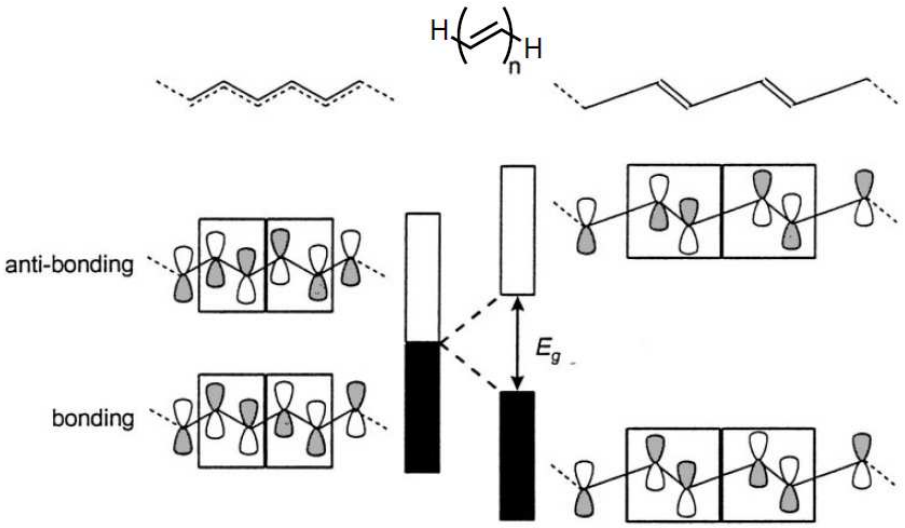

Figure 2.6 *Band gap formation by localization of double bonds in polyacetylene [14].*

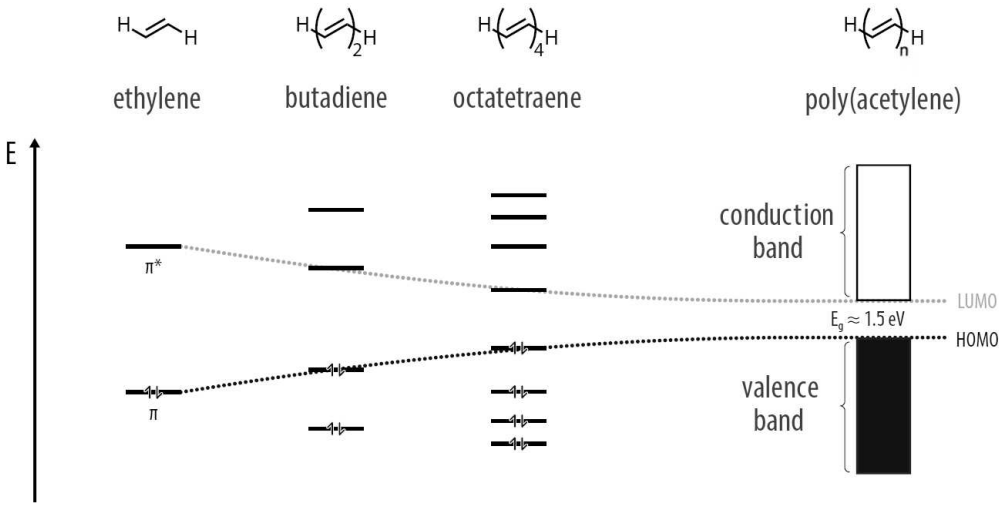

Figure 2.7 *Energy bands formation as the number of polymerization increases [13].*

As depicted in Figure 2.7, polyacetylene has a band gap of about 1.5 eV comparing to 1.1 eV for Si and 1.4 eV for GaAs [1]. Although, neutral polyacetylene is a poor semiconductor. As discussed in subsection 2.2.3, dopants can be used to enhance its conductivity.

Although, polyacetylene is a historically important material, but the conjugation can be quite different from the other conjugated polymers with amines or aromatic bonds instead of carbon doubles. Also, there is a bit of controversy in the field about whether most organic semiconducting polymers, especially amorphous ones, should be treated in a band model or if it is better to talk about HOMO and LUMO and some delocalization. However, the discussion can be continued based on polyacetylene.

2.2.3 Charge generation and transport within conjugated polymers

The mechanism of current conduction in conjugated polymers is different from inorganic semiconductors both from the charge generation and the charge transport viewpoint.

Charge generation

The formation of charge carriers on organic semiconductors can be explained by examining the resonance forms of conjugated molecules. For instance, polyacetylene has two energetically and geometrically equivalent resonance forms known as the degenerate ground states [15], shown in Figure 2.8. It can be seen that the lower energy ground states are more stable than the higher energy delocalized one leading to the Pierels' distortion of the unstable deloclized one towards the ground states, as discussed before in section 2.2.

These two ground states can coexist on the same backbone chain with a boundary between them as the consequence of lattice defects. A certain density of the lattice defects can exist even with a small thermal excitation [9]. The lattice defects lead to spontaneous formation of neutral *solitons*. The lattice defect, or the solitonic defect, associated with a domain boundary is shown in Figure 2.9a for polyacetylene. In chemistry point of view, neutral solitons are delocalized radicals (delocalized over seven carbon atoms): They do not carry charge (q = 0), but they have spin (s = ½). Neutral solitons do not contribute to conduction since they have no charge, but they result in an extra energy level in the band gap with limited delocalizatin, as illustrated in Figure 2.9b.

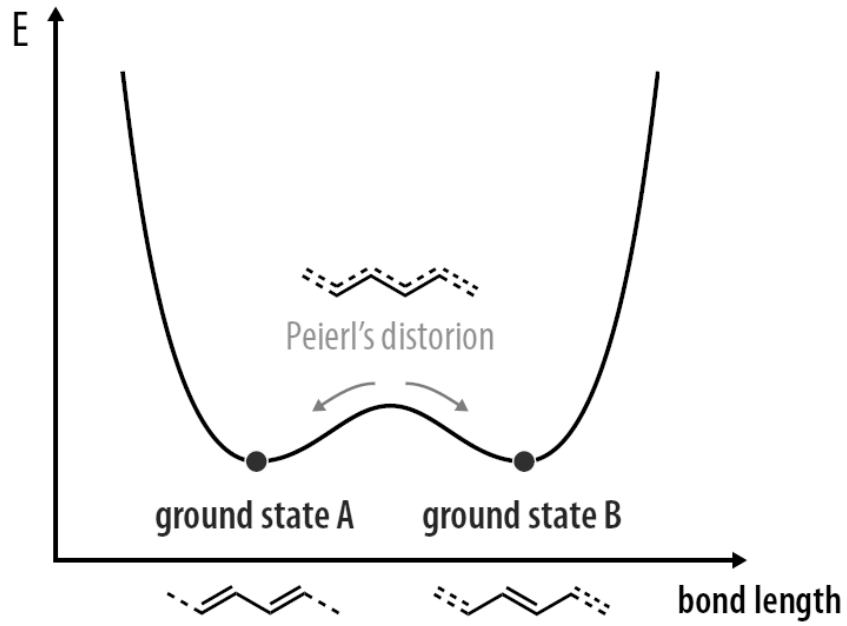

Figure 2.8 *Energy levels for the two ground states of polyacetylene ([13], modified).*

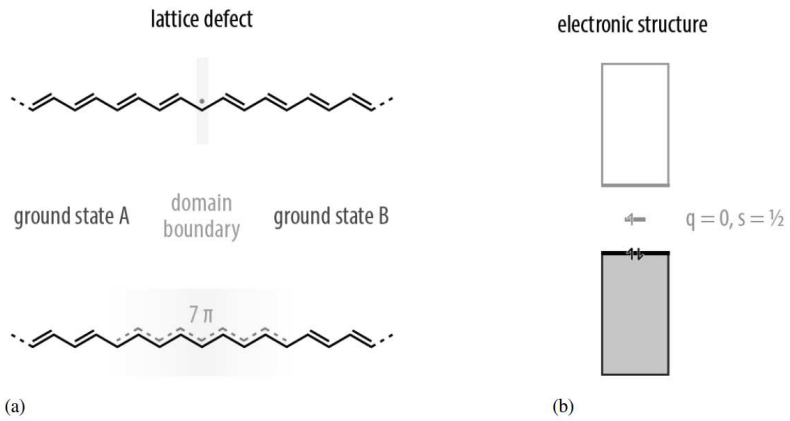

Figure 2.9 *Lattice defect results in (a) neutral soliton fomatin, and (b) an extra energy level in the band gap of polyacetylene [13]*

Undoped polyacetylene in the crystalline state is a poor semiconductor. The polyacetylene in the crystalline state can become semiconducting or even metallic by a chemically doping process. The dopant induce no chemical reaction, and acts as a single electron donor (reductant) or acceptor (oxidant). The n-type doping can be achieved by reductants such as Na, K, Li, and p-type doping can be done by oxidants such as I_2, AsF_5, SbF_5 [13]. The chemical doping increase the conductivity and the charge carrier mobility by several orders of magnitude.

The chemical doping converts neutral solitons into positive or negative soliton charge carriers. Figure 2.10 schematically shows the formation of the positive and negative charge carries. The positive or negative solitons possess no spin (s = 0), but they have charge q = +e or -e, respectively. As Figure 2.10 shows, the positive and negative solitons form isolated charge carriers with limited delocalization on an extra energy level in band gap. More doping level first results in more isolated positive solitons with still limited delocalization, but gradually as the dose of dopants increases, solitanic defect states interact with each other leading to narrow band negative or positive solitans in the band gap. It means that high levels of doping make polyacetylene a metallic conductor.

Charge transport

The transport of charge carriers in conjugated polymers typically follows a hopping mechanism and is modeled similar to highly disordered systems. The hopping transfer is based on the thermal excitation of the electrons, and it depends on the temperature and the molecular thermal vibrations [9]. Actually, the thermal hopping between finite chains of conjugated polymers dominates their microscopical conductivity. This hopping process plus the transport of positive or negative solitons through the polymer chain limit the charge carrier mobility in organic semiconductors. Moreover, the conductivity of stretch-oriented conjugated polymers is higher in the stretch direction than perpendicular to it. These characteristics brings them a highly anisotropic conductivit [5].

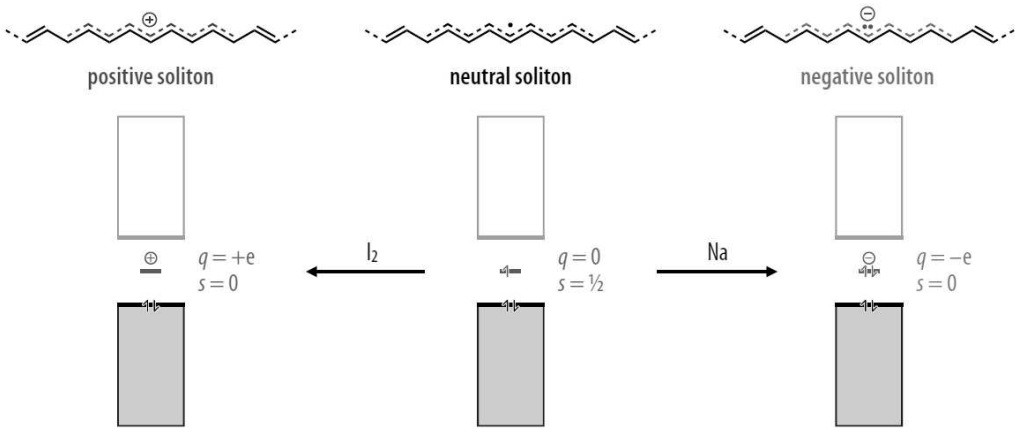

Figure 2.10 *Formation of positive or negative soliton charge carriers [13].*

Polyacetylene as a degenerate ground-state polymer is the simpler to model comparing to nondegenerate ones. The nondegenerate ground-state polymers have no degeneracy in the ground-state energy. Instead, the interchange of single and double bonds yields two states of different energies [16]. In lieu of solitonic defects, these nondegenerate ground-state energies lead to *polaron* or *bipolaron* states for charged defects [16]. Most of the conjugated-polymers have cyclic π-conjugated backbone chain in stead of a linear one. Some of the other common conjugated polyemers are arranged in Table 2.1.

Table 2.1 *Different conjugated polymers ([17], modified)*

Polymer (date conductivity discovered)	Structure	Band gap (eV)	Conductivity# (S/cm)
I. Polyacetylene and analogues			
Polyacetylene (1977)	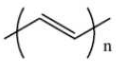	1.5	$10^3 - 1.7\times10^5$
Polypyrrole (1979)	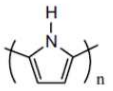	3.1	$10^2 - 7.5\times10^3$
Polythiophene (1981)	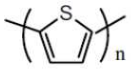	2.0	$10 - 10^3$
II. Polyphenylene and analogues			
Poly(paraphenylene) (1979)	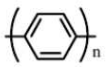	3.0	$10^2 - 10^3$
Poly(p-phenylene vinylene) (1979)	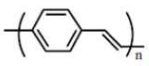	2.5	$3 - 5\times10^3$
Polyaniline (1980)	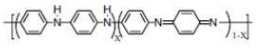	3.2	30 – 200

The range of conductivities listed is from that originally found to the highest values obtained to date (after Dai, 1999, copyright 1999 Marcel Dekker, Inc.)

3. ORGANIC METAL-SEMICONDUCTOR DIODES

The organic MS diode, also called an organic Schottky diode, is introduced in this section. It is instructive to first have an overview of the device structure and the fabrication processes in order to appreciate device physics. then, the operation of the organic Schottky diode under equilibrium and steady state conditions are discussed followed by how to characterize and model the organic diode. Finally, the performance of the diode under rectification as a fundamental function in electronic circuits is presented.

3.1 Fabrication of organic MS diodes

The fabrication process of the organic Schottky diodes in this work is based on the methods that mimic high-throughput roll-to-roll processes. The roll-to-roll processing, also known as web processing, reel-to-reel processing or R2R, is the process of fabricating electronic devices on a roll of flexible plastic. Indeed, the ongoing development of the organic semiconducting materials facilitate the fabrication of electronic devices on flexible substrates utilizing methods compatible with the solution processing techniques. This compatibility leads to high volume and low cost productivity.

The roll-to-roll processing technique enables the roll of material to be coated or printed using different thermal evaporation techniques or different printing techniques, respectively. Thermal evaporation in vacuum allows for deposition of purified materials, whereas printing in ambient conditions results in contaminated amorphous thin films. In this section, different printing techniques along with different thermal evaporation techniques are presented, however the main focus is on e-beam evaporation and gravure printing techniques. It is also beneficial to inspect the device structure first.

3.1.1 Device structure

The organic Schottky diode is composed of two metal electrodes and an organic semiconductor thin film sandwiched amid the metal contacts. In the printed electronics, it is more preferable to fabricate the organic diodes with a vertical sandwich structure due to the ease of fabrication in comparison with the lateral printed structure. However, the organic diodes with lateral structures have also been reported in the literature as in the work of [18, 19].

In this work, the diodes are fabricated vertically. The two-terminal sandwich structure is presented in Figure 3.1.

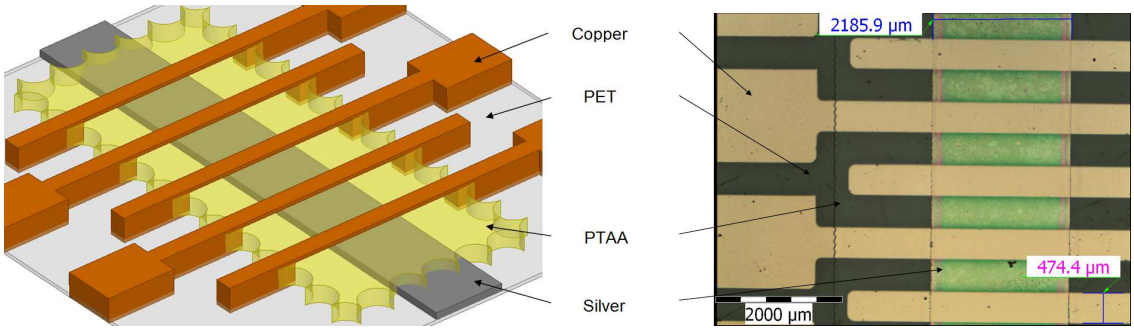

(a) (b)

Figure 3.1 *(a) The diode structures, and (b) the microscopic image of the 1mm^2 (2mm×0.5mm) diodes. Dimensions in (a) and (b) are not compatible.*

As Figure 3.1 illustrates, the organic Schottky diode in this work consists of silver and coppers as the metal contacts enfolding the Poly(triarylamine) (PTAA) as the organic semiconductor, where all these thin films have been layered successively on flexible poly(ethylene terephthalate) (PET) film. The thickness of the gravured semiconductor layer varies from 400nm to 500nm and the diode area is 1mm^2. The thicknesses of the thermally deposited silver and copper layers are 100nm. Figure 3.1 shows that several copper contacts has been coated to increase the probability of yielding workable diodes and to avoid possible unexpected failures during measurement.

The fabrication techniques limit the range of the possible materials utilized in manufacturing the proposed organic Schottky diode. First, the substrate is required being flexible, chemically resistant and capable to withstand the processing temperature. Second, the semiconductor material needs to be air stable, soluble in a suitable solvent and processable using gravure printing technique. Third, the electrical properties (e.g. mobility, dielectric constant and conductivity) of the materials are supposed to be appropriate to assure the functionality of the printed diode.

Substrate

Polyster films are regularly used as the substrate in the printed electronics. The flexibility of the plastic substrates give them an advantage over the silicon based substrates, and makes them suitable for roll-to-roll production. The polyster films such as PET and poly(ethylene naphthalate) (PEN) exhibit high transparency, relatively high surface smoothness and good thermal and mechanical properties. These are the properties which are not achievable by paper or thin metal foils as the alternative candidates.

The substrate used in this work is heat-stabilized PET, ST506 from Dupont Teijin Films: a thermoplastic semi-crystalline plastic film with a glass transition temperature T_g of 78°C [20]. In spite of the relatively low T_g, the heat-stabilization process improves the dimensional stability of the film allowing processing temperature up to 150°C [21].

Semiconductor

Organic conjugated polymers can be prepared for solution processing by adding flexible side chains to the polymer backbone to improve solubility. However, they usually exhibit mobilities far less than 1 cm^2/Vs due to disorder and impurites, which reduce the electronic coupling between neighboring molecules.

PTAA is an amorphous p-type organic semiconductor which has a reported (lateral) charge carrier mobility of 2×10^{-3} cm^2/Vs [22]. Figure 3.2 illustratest the repeat unit of PTAA. The PTAA possesses good stability, which makes it capable of being processed in ambient conditions. This will reduce its major disadvantage of low hole mobility. Furthermore, PTAA is fully amorphous meaning that it does not form crystals in the printing or dying processes [21]. This property augments the reproduciblilty of the semiconucting layers in the printed diodes.

The PTAA used in this work was obtained in solution from Merck Chemicals Ltd, and was printed using a laboratory-scale automatic gravure printing press, Labratester Automatic from Norbert Schläfli Maschinen. All layers were cured at 115°Cfor 5 minutes.

Conductors

In printed electronics, thick layers of conductors can be applied using either screen or gravure printing of flake inks. whereas, thin films (several ten nanometers) of conductors are deposited either by vacuum evaporation or sputtering. Printable conductive inks usually consist of either large silver flakes/spheres leading to high viscosity paste inks which are especially suitable for screen printing, or silver nanoparticles resulting to low viscosity inks appropriate for gravure printing.

For organic Schottky diodes, silver paste contact and sputtered copper contact have been reported in the literature [23]. Furthermore, the use of organic conductors such as polyanilline and poly(3,4-ethylenedioxythiophene):poly(styrenesulfonate) (PEDOT:PSS) have been reported [24, 25]. In this work, thin (100nm) copper and silver layers are deposited using e-beam evaporation technique. The contact pattering is done through shadow masking.

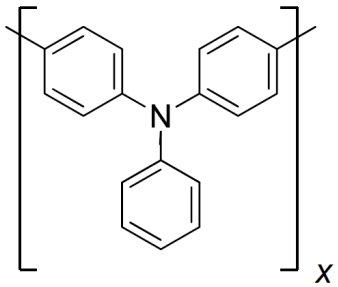

Figure 3.2 *The repeat unit of unsubstituted poly(triarylamine). x denotes the number of polymerization [21].*

3.1.2 Thermal evaporation

Deposition of purified materials is possible with different thermal evaporation techniques in vacuum. The target material is placed into a vacuum chamber and heated utilizing different heating systems. Once the vapor pressure of the heated material exceeds the pressure of the background gases in the vacuum chamber, the material evaporates and condenses on the cooler target surfaces. Organic semiconductors with high molecular weight cannot be deposited this way since they are too heavy to evaporate. In fact, heavy organic polymers decompose to small molecules instead of evaporating with this technique. In this work, thermal evaporation has merely used for coating metal contacts.

Thermal evaporation of metals is typically performed under high or ultra high vacuum conditions. This is done for several reasons. First, the evacuation of the chamber reduces the partial pressure of oxygen or other background gases. These gases might contaminate the sample or even react with the heating apparatus. Second, metals usually possess low vapor pressure. Vacuum conditions permits these low vapor pressure materials to evaporate. Finally, the mean free path of the evaporant particles is extended to larger than the source-to-substrate spacing. This allows the source material to travel to the substrate without deflection caused by intermolecular collisions.

The mean free path (λ) of a gas (as a collection of particles that collide elastically with each other) is given by:

$$\lambda = \frac{kT}{4\pi\sqrt{2}r^2p}, \tag{3.1}$$

where k[J/K] is the Boltzmann constant, T[K] is the temperature, p[Pa] is the pressure, and r[m] is the effective molecular radius of the gas.

A typical mean free path for air at room temperature is 65nm [9]. Therefore, the evaporated materials at atmospheric pressure scatter many times with no appreciable traveled distance. This results in the lost of their directionality. Typical pressure for vacuum thermal evaporation falls in the range of 10^{-6}-10^{-8}[Torr] [9]. For these pressures, the typical mean free path is on the order of meters or longer. For instance, the mean free path is approximately 5km at 10^{-8}[Torr]. With this mean free path, the particles of the evaporant material travel in a line-of-sight pattern from the source to the substrate.

In addition to the mean free path, the composition of the background gases during the deposition exerts a strong influence on the results of the thermal evaporation process. In fact, Some evaporants (especially reactive metals) react with gases which are present in the vacuum chamber. As the evaporant is being heated, its reactions with water, oxygen, hydrogen, and other background gases are accelerated. A clear indication is the reduction in the pressure of the chamber while the material is being evaporated. These reactions could change the properties of the deposited films. For instance, It has been shown that organic semiconductors can be doped by these background gases [26].

It should be noted that additional sources of background gases appear through des-

orption of gases from the source material, crucible, filaments, and other surfaces in the vacuum chamber, once heating of the source material begins. these gases can come from the volatile materials incorporated in the source material or the thermal decomposition products.

In this work, Electron beam (e-beam) evaporation is used to deposit metal contacts of the diode. Actually, the e-beam evaporation technique is suitable to evaporate materials with high evaporation temperature such as metals, glasses, and ceramics. This technique is not applicable to Organic semiconductors, which have substantially lower evaporation temperatures [9].

electron beam evaporation

E-beam evaporation is a process analogous with thermal evaporation: the source material is heated above its sublimation temperature and evaporated to form a thin film on the surfaces that is stroke by the evaporant particles. However, the source material is heated through the bombardment with an electron beam emitted from a charged tungsten filament under high vacuum conditions. In fact, A heated filament emits high voltage electrons thermionically, and magnetic elements focus and steer the launched beam onto the source material contained in a crucible. The impacting electrons cause substantial heating in the substrate via losing their kinetic energy causing the target atoms to transform into the gaseous phase. These atoms then coat the inner wall of the vacuum chamber with a thin layer of the source material. Figure 3.3 shows a cross-section of the different parts of an e-beam evaporator.

Electron beam deposition can reach extremely high temperatures, well over 3500°C, which permits the evaporation of the materials with very high evaporation points. Tolerating high temperatures, appropriate crucibles for different source materials are recommended by manufacturers. High purity of deposited films can be achieved due to the low contamination of the source material, which is in turn because of high vacuum and low contact of the melt with the crucible.

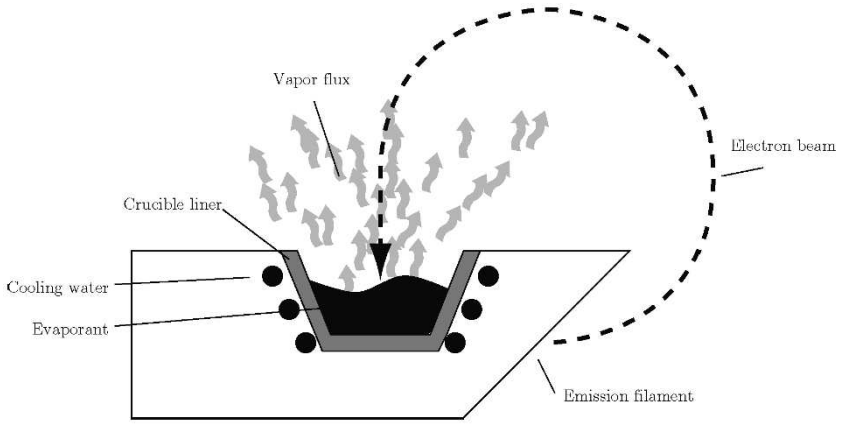

Figure 3.3 *Schematic cross-section of an e-beam evaporator [9].*

The e-beam evaporation technique deposit the source material on a large area. Thus, it is needed that the unwanted material to be defined and removed in a subtractive process. It means that the deposited thin films usually need to be patterned. In fact, it is necessary to pattern the metal contacts of the organic diode using another technique. Among different pattering techniques, the shadow masking is used during evaporation so that the material is merely deposited where it is wanted.

In shadow masking, a stencil intercepts unwanted material and allows the desired material to coat the substrate. The shadow mask can be a free-standing or sheet like an etched metal foil, or a patterned layer on the substrate which can be easily removed. The size of the intended features limit the feasibility of the process.

A noticeable advantage of e-beam evaporation over thermal evaporation is the possibility to add more energy into the source material, which yields a higher density film with an increased adhesion to the substrate. Also, a lower degree of contamination from the crucible exists than in the case of thethermal evaporation since the electron beam only heats the source material and not the entire crucible. Furthermore, several different materials can be deposited by using a multiple crucible E-beam gun without breaking the vacuum.

On the other hand, several potential disadvantages for e-beam evaporation can be noticed. First, Samples can experience a significant flux of reflected electrons, which can charge or disrupt some materials. Second, the background pressure must be held low to avoid rapid oxidation of the filament. Third, The hot substrate can emit a substantial IR and UV radiation via blackbody emission, as well as some Bremsstrahlung x-ray radiation [9]. Finally, The technique is restricted to materials which have a high decomposition temperature to tolerate electron bombardment.

3.1.3 Printing

Traditional printing methods used in printed media can be used as a production method in printed electronics. The required film thickness and the pattern resolution defines which printing technique to be utilized for different applications. Printing technologies can be classified as contact and non-contact methods, depending on whether a physical contact between the printer and the substrate surface exists or not. As commonly used contact mode printing methods, gravure printing, flexography printing and screen printing can be named. Non-contact digital inkjet printing technology has also been intriguing for fabrication of printed electronic devices due to the free operation of the printing plate, high variability of the printed patterns and high resolution. All these techniques are suitable for roll-to-roll processing and high volume production.

In order to gain high quality printed patterns, it is essential to optimize the inks for different printing techniques. In fact, the ink should be formulated for each printing process and each printing substrate separately. For instance, the rheological properties of the ink

determines the printing quality. Among these rheological properties, the most important ones are the ink viscosity and surface energy. Low viscosity materials are suitable for inkjet printing, whereas medium and high viscosity inks yield good results in gravure and screen printing, respectively [27]. The surface energy of the ink determines how evenly the ink dries during the drying process. Choosing right solvents (or a solvent mixture) and adding different binders or additives can modify these properties of the ink.

However, Organic semiconductors are also sensitive to the additives used to modify the ink viscosity and improve the printing quality. They influence the electrical properties of the organic semiconductors. The drying process also has an effect on the electrical properties of the ink, and usual UV curing methods cannot be used during drying process.

In addition, increasing the solubility of the organic conjugated polymers sets some restrictions and challenges on the performance of the material. Actually, most of the materials with excellent solubility form amorphous films, and the electrical performance of the disordered amorphous materials is not comparable with the crystalline materials. However, the reproducibilty of the organic printed devices with amorphous thin films will increase.

Some semicrystalline organic semiconductors have been successfully to fabricate inks for printing purposes [28] However, the reproducibility of the devices is challenging because of the irregular crystal formation in the printed layers [29].

Gravure printing

Gravure printing is a mechanical printing method utilizing engraved cylinder or plates as the pattern carriers. In fact, the printing patterns are engraved as a collection of tiny cells on the surface of gravure cylinders or plates. Figure 3.4 shows both type of the engraved surfaces used during gravure printing. The ink collects in the gravure cells, while the excess ink being scraped from the non-pattern areas by a doctor blade. The substrate is passed through a nip formed between a rubber-coated impression cylinder and the gravure cylinder or plate. Then, the ink is transferred by a combination of capillary action and the pressing of the substrate into the engraved cells, helped by the rubber surface of the impression cylinder.

Either gravure plates or gravure cylinders can be used for sheet-fed or roll-to-roll printing, respectively. In this work, the PTAA semiconductor layer is fabricated using s sheet-fed gravure printing press, as depicted in Figure 3.4b.

Fast throughput, consistency and high quality printed results make the gravure printing an intriguing option for long production runs. The thicknesses of the dried layers are in the order of hundreds of nanometer to a few micrometer, suitable for the thin film transistors, diodes and capacitors. The required viscosity of the ink is within moderate levels, in the order of tens to 100 mPa.s, which lowers the solid content of the ink and removes the need for additives.

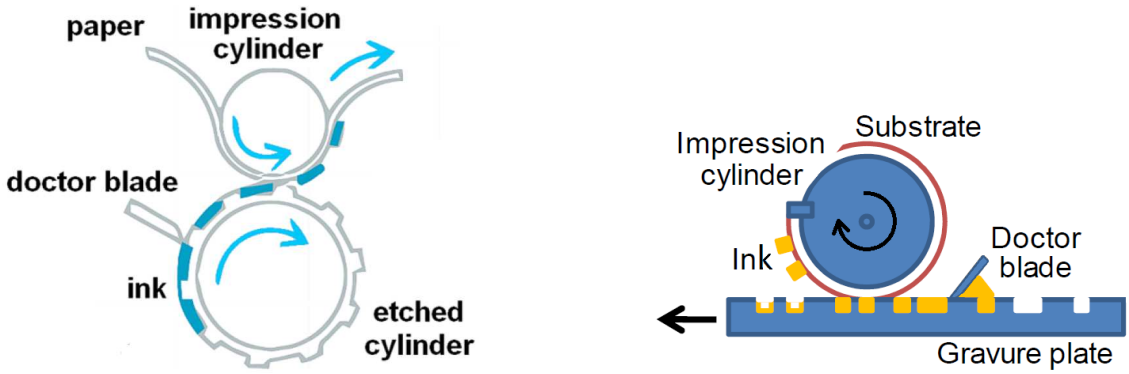

(a) (b)

Figure 3.4 *(a) Roll-to-roll gravure printing process using a gravure cylinder [21], and (b) sheet-fed gravure printing process using a gravure plate [21].*

Using gravure printing method, the patterns and images are pixelated consisting of individual dots. Different levels of darkness are produced by varying the area and depth of the cells, which is called the halftone technique. The transferring process of the ink from the gravure cups onto the substrate is illustrated in Figure 3.5. while the image goes down pixelated by the pits, levelling is critical to get a smooth, pinhole-free layer. The pixelated patterns influence the functionality of the device since electronic devices and circuits require continuous and consistence paths.

One of the main disadvantages of gravure printing in printed electronics is the expenses of the process. large reservoirs of the inks significantly increase the cost of the printing. Furthermore, high accuracy engraving methods requires significant costs in order to produce precisely defined tiny individual cups onto the gravure cylinders or plates. It results in relatively expensive gravure surfaces.

In comparison to the other printing processes, Gravure printing facilitates the printing of high quality pinhole free layers suitable for various electronic applications including OLEDs [30], transistors [31], solar cells [32] and rectifying diodes [33]. It is due to the fact that gravure printing is capable of transferring more ink onto the substrate in comparison to the other printing processes. However, the contamination of the printed materials is higher because of the contact mode printing process and ink spreading method. These contamination might disturb the performance of the fabricated devices.

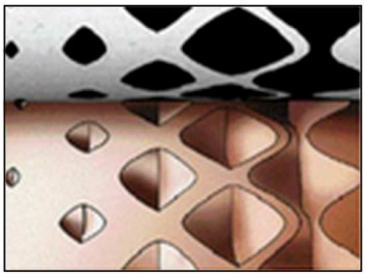

Figure 3.5 *Pixelated ink transfer from the gravure cups onto the substrate [21].*

Flexography

Flexography or flexographic printing is frequently used for printing on plastic, foil, acetate film, brown paper, and other materials used in packaging. This method of printing is suitable for printing on flexible plates made of rubber or plastic. Flexography utilizes embossed printing patterns instead of the engraved patterns used in the gravure printing method. In fact, The inked plates with a slightly raised images are rotated on a cylinder which is in contact with the substrate, and the patterned image transfers to the substrate. Flexography is a high-speed printing process used for printing on many types of absorbent and non-absorbent materials to produce continuous patterns.

The flexographic printing benefits from lower risk of ink contamination on the substrate due to the embossed structures instead of the engraved ones. In fact, the printing plate touches the substrate merely at places where the ink is transferred. The shape of the embossed structure is the other benefit of the flexography: patterns with uniform smooth edges can be embossed on the printing plates, which facilitates smooth edges and patterns on the printed layers. In contrast, the engraved or meshed cells used in gravure and screen printing, respectively, reduce the smoothness of the pattern edges. The smoothness of the edges affect the operation of the printed devices with small dimensions. In printed electronics, flexography is used in fabrication of printed devices such as solar cells [34], OLEDs [35], passive components and electrodes [36].

Screen printing

Screen printing is a technique in which an ink-blocking stencil is attached to a finely-woven mesh screen. The attached stencil forms open areas of mesh which transfer a thick paste ink to make a sharp-edged image onto the substrate. The ink is forced through the stencil by moving a fill blade or squeegee across the screen stencil to transfer the ink through those areas not covered by the stencil. The screen printing can be used to print on a wide variety of substrates with different shapes, thicknesses and sizes. The substrates include paper, paperboard, plastics, glass, metals, fabrics, and many other materials.

High viscosity of the ink requires that the ink contains relatively high solid content and suitable additives. High solid content and additives lead to thicker films, which consequently make problems for the device operation. Due to the relatively thick dry layers, screen printing is utilized to fabricate electronic circuit boards [37], electrodes [38], current grids [39] and RFID antenna [40].

Inkjet printing

Inkjet printing technology is a type of printing technique, where tiny droplets of liquid ink are propelled onto paper or other substrates. The continuity of the single droplets limit the functionality of this technology in printed electronics. In fact, the conductors and

dielectric layers have to be continuous and uniform for proper functionality. In printed electronics, various functional materials such as conductors [41], semiconductors [42] and dielectrics [43] can be utilized using inkjet printing technology.

Inkjet printing technology can be classified into two main types based on the method used to deposit the ink: drop-on-demand and continuous inkjet. In drop-on-demand mode, the droplets are generated when required, whereas in continuous mode a stream of droplets is generated continuously.

The inkjet technology enables a digital process, in which the printed patterns can be easily modified using optional computer software and changing the print file. Also, the contamination of the printed patterns are minimal due to the non-contact operation.

3.2 Schottky and ohmic contacts

When a metal and a semiconductor joined, two possible types of contact can result depending on the types of the metal and semiconductor. The contact may be either rectifying, which only allows current to pass in one direction, or ohmic, in which current can pass in either direction. This section deals with both the rectifying and ohmic contacts, and the discussion is totally around the p-type semiconductor since PTAA is p-type.

rectifying contact

Before discussing the behaviour of a metal-semiconductor contact, it is necessary to introduce the concept of the work function. The work function ($q\Phi$) of a material in the vacuum is the energy required to remove an electron at the Fermi level (E_F), the level of the electrochemical potential for the electrons, to the vacuum outside the material. The values of work functions are very sensitive to surface contamination. Typical values for very clean surfaces are 4.3 V for Al and 4.8 V for Au [1].

When a metal with work function $q\Phi_M$ is brought in contact with a p-type semiconductor having a work function $q\Phi_S$, the transfer of positive charge from the semiconductor to the metal occurs until the alignment of the Fermi levels at equilibrium happens (Figure 3.6). For $\Phi_M < \Phi_S$, the semiconductor Fermi level is initially lower than that of the metal before contact is made. To align the two Fermi levels, the electron energies of the semiconductor must be raised relative to that of the metal. It results in the form of a constant equilibrium potential difference V_0 between the semiconductor and the metal across some region W about the junction. The region W is called the depletion region, and the potential difference V_0 is called the contact potential.

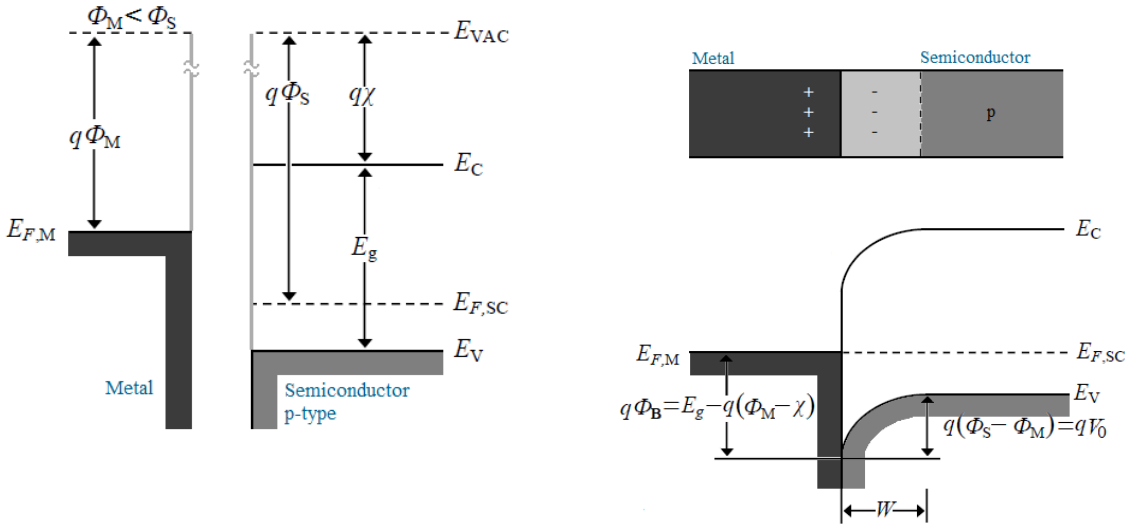

(a) (b)

Figure 3.6 *Schottky barrier between a p-type semiconductor and a metal having a smaller work function: (a) band diagrams before joining; (b) band diagrams for the junction at equilibrium. E_{VAC} is the vacuum energy level, $q\Phi_M$ is the metal work function, $E_{F,M}$ is the metal Fermi energy, $E_{F,SC}$ is the semiconductor Fermi energy, $q\chi$ is the semiconductor electron affinity, E_C is the semiconductor conduction band edge, E_C is the semiconductor valence band edge, $q\Phi_B$ is the Schottky barrier energy, W is the depletion region and V_0 is the contact potential.*

Indeed, the transfer of positive charge form the p-type semiconductor to the metal results in a depleted region W at the semiconductor near the junction. W is called depletion region since it is almost depleted of carriers compared with the rest of the semiconductor, and almost only space charge exists within W because of uncompensated acceptor ions. The negative charge due to the uncompensated acceptor ions within W matches the positive charge on the metal. By assuming the negative charge in the metal is a thin sheet of charge to the left of the junction, the depletion width W in the semiconductor is given by:

$$W = \sqrt{\frac{2\epsilon_0\epsilon_r(V_0 - V)}{qN_A}}, \tag{3.2}$$

where ϵ_0 is the permittivity of vacuum, ϵ_r is the relative permittivity of the semiconductor, V_0 is the contact potential, V is the external applied voltage, q is the elementary charge and N_A is the density of dopants.

Within the depletion region, holes are in transit from one side of the junction to the other. Some holes diffuse from the semiconductor to the metal, and some are swept by the electric field from the metal to the semiconductor. The equilibrium contact potential V_0 prevents further net hole diffusion from the semiconductor conduction band into the metal and is equal to the difference of work function potentials $\Phi_M - \Phi_S$.

By definition, the potential difference V_0 is an equilibrium quantity, and no net current can result from it. It is a built-in potential barrier, which is necessary to the maintenance

of equilibrium at the junction; it does not imply any external potential. However, the V_0 can be decreased or increased by the application of either forward- or reverse-bias voltage V across the junction.

The Schottky barrier height Φ_B for electron injection from the metal into the semiconductor conduction band is predicted by Schottky-Mott model and is equal to ${}^{E_g}/_q - (\Phi_M - \chi)$, where $q\chi$ is called the electron affinity and is measured from the vacuum level to the semiconductor conduction edge. The Schottky-Mott model predicts the existence of the band bending and the formation of the Schottky barrier in metal-semiconductor junctions. That is why the rectifying contact is also called the Schottky barrier contact.

when a forward-bias voltage V is applied to the Schottky barrier of Figure 3.6b, the contact potential is reduced from V_0 to $V_0 - V$ (Figure 3.7a). As a result, holes in the semiconductor valence band can diffuse across the depletion region to the metal. This gives rise to a forward current (semiconductor to metal) through the junction. Conversely, a reverse bias increases the barrier to $V_0 + V_r$, and hole flow from semiconductor to metal becomes negligible (Figure 3.7b). In either case flow of holes from the metal to the semiconductor is retarded by the barrier Φ_B, which is not affected by the bias voltage. The resulting diode current is suggested in Figure 3.7c. The reverse saturation current (I_0) depends on the size of barrier Φ_B for hole injection from the metal into the semiconductor. then, the Schottky barrier diode can rectify, with easy current flow in the forward direction and little current in the reverse direction. The current-voltage characteristics is discussed in section 3.3.

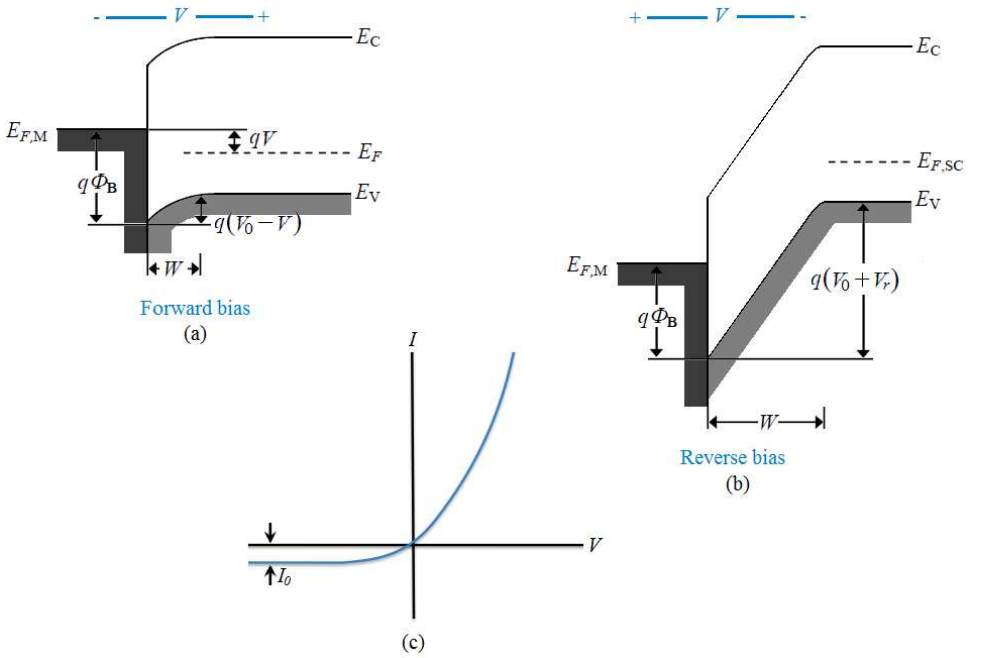

Figure 3.7 *Effects of forward and reverse bias on the junction of Figure 3.6: (a) forward bias; (b) reverse bias ($V = -V_r$); (c) typical current-voltage characteristic.*

The forward current is due to the injection of the majority carriers from the semiconductor into the metal with no minority carrier injection, and the storage delay time associated with the minority carrier injection is absent in Schottky barrier diodes. Thus, this type of diode is essentially a majority carrier device, and their high-frequency properties and switching speed are generally better than typical p-n junctions.

Ohmic contact

It is important that the metal-semiconductor contact which connect the diode to the electronic circuit to be an ohmic contact. This is due to the fact that the ohmic metal-semiconductor contact, which has a linear IV characteristic in both biasing directions, possess minimal resistance and no tendency to rectify signals.

For an ohmic metal-semiconductor contact, the charge transfer in aligning the Fermi levels occurs from the metal to the semiconductor. For a p-type semiconductor, this happens when $\Phi_M < \Phi_S$, where the Fermi levels are aligned at equilibrium by transferring holes from the metal to the semiconductor. This lowers the semiconductor energy levels relative to the metal at equilibrium (Figure 3.8b). In this case the barrier to hole flow between the metal and the semiconductor is small and easily overcome by a small voltage. Unlike the rectifying contacts, no depletion region occurs in the semiconductor since the electrostatic potential difference, required in Fermi levels alignment at equilibrium, needs that the hole accumulates in the semiconductor.

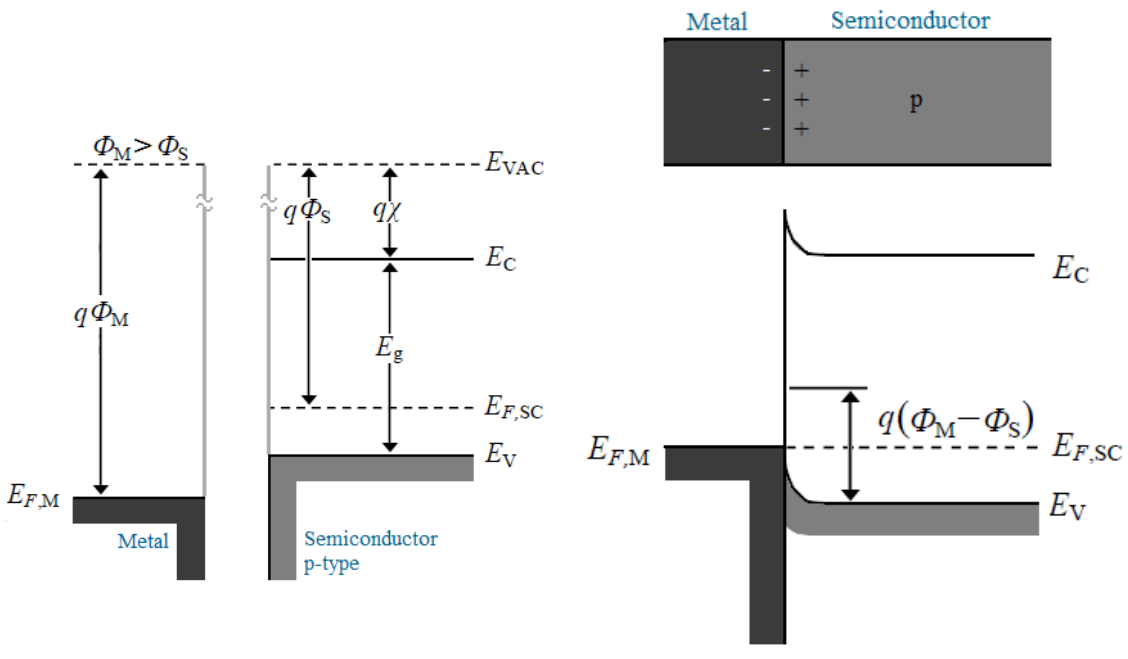

(a) (b)

Figure 3.8 *Ohmic contact between a p-type semiconductor and a metal having a greater work function: (a) band diagrams before joining; (b) the equilibrium band diagram for the junction.*

The Schottky-Mott model correctly predicts the existence of band bending for different semiconductors; however, its prediction of the Schottky barrier height is not compatible with the experimental measurements. In fact, the center of the semiconductor is locked or pinned to the Fermi energy level of the metal due to a phenomenon called *Fermi level pinning*. Thus, the Schottky barrier height is almost equal to $E_g/2$ and insensitive to the metal and semiconductor work functions.

The Fermi level pinning occurs due to chargeable energy states inside the band gap of the semiconductor right at the interface. These energy sates either are induced during the direct chemical bonding of the metal and the semiconductor (metal-induced gap states) or are already present on the surface of the semiconductor (surface states).

For organic semiconductors, the Schottky model can be modified by considering the HOMO and LUMO levels instead of the valence and conduction bands, respectively. In addition, the conjugated polymers, as typically used in organic light-emitting diodes or solar cells are undoped semiconductors with trap states. Then, the Fermi level pinning due to interface trap states results in a constant Schottky barrier potential in organic semiconductor-metal interfaces. these properties of the organic semiconductors change the alignment of the energy levels throughout the device.

Applying the equation 3.2 for an organic semiconductor, N_A can be equated to the density of free charge n [44]. The undoped polymeric organic semiconductors usually exhibit low density of charge carrier concentrations. Thus, the depletion region can expand throughout the thickness of the semiconductor, according to the equation 3.2. It means that the semiconductor is fully depleted, and the depletion width do not change significantly by biasing voltage. In fact, the organic Schottky diodes should be considered as metal-insulator-metal (MIM) diodes instead of voltage controlled metal-semiconductor diodes.

Therefore, when electrodes with different work functions are utilized, a diffusion potential V_d (the counterpart of the contact potential V_0), which corresponds to the work function difference between the anode and the cathode, forms across the undoped semiconductor. Accordingly, the diffusion potential only depends on the nature of the electrodes and not on that of the semiconductor layer. The diffusion potential equals to the barrier height Φ_B. The anode acts as the ohmic injecting contact, and the cathode acts as the non-ohmic (rectfying) collection contact.

In MIM structures, band bending due to the uncompensated dopants is absent. Also, the injected holes at the ohmic contact do not result in band bending at the semiconductor near the interface. In fact, once the organic semiconductor and the metal are brought into contact, the Fermi levels align by transfer of charge from the electrode with higher work function (injecting contact) to the electrode with the lower work function (collection contact). Thus, the energy levels can be illustrated with tilted, rigid energy bands, as depicted in Figure 3.9.

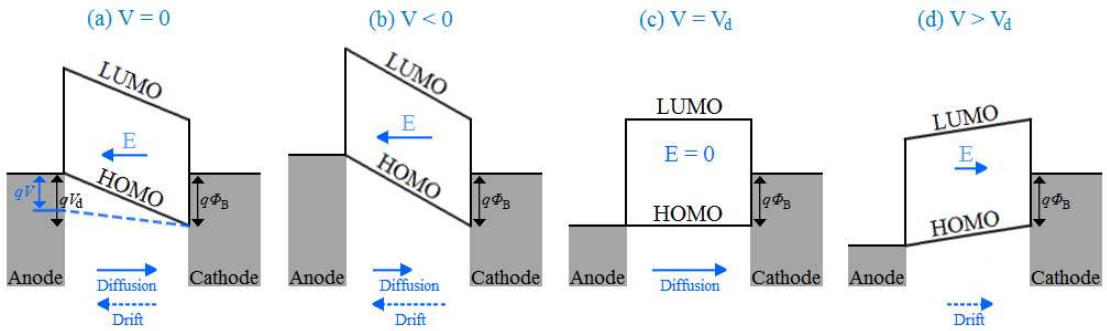

Figure 3.9 *Energy diagram of an organic diode with a fully depleted undoped p-type semiconductor for (a) thermal equilibrium and upon applying a small positive bias smaller than the built-in voltage (dashed line), (b) reverse biasing, (c) forward biasing voltage equals to contact potential, and (d) forward biasing voltage greater than contact potential. E is the electric field.*

Applying an external biasing voltage can either increase (reverse biasing, Figure 3.9b), or decrease (forward biasing, Figure 3.9c and 3.9d) the injection barrier. When no voltage is applied, the work function difference induces an electric field that inhibits any hole injection at the anode, and the Fermi energy levels of the anode and the cathode align (Figure 3.9a). For reverse biasing, this backward electric field increases, so that no current is expected to flow through the diode. The electric field is cancelled by the application of a voltage that exactly compensates the diffusion potential; this corresponds to the situation of flat bands (Figure 3.9c). When $V > V_d$, the electric field is reversed and current starts to flow through the diode (Figure 3.9d). In fact, the positive charge carriers are transferring from the injecting anode contact to the HOMO of the semiconductor, from where they move to the rectifying cathode contact.

As long as the semiconductor is fully depleted, the electric field is constant across the whole semiconductor. the direction of the electric field determines the slope of the tilted energy levels, and also shows the direction of the drifted charge carriers. However, the diffusion current might occur due to the different concentrations of the charge carriers. Thus, the total current is the sum of the drift and the diffusion of the charge carriers. The current contributions are discussed in section 3.3.

The performance of the injecting anode contact and the rectifying cathode contact can be improved by manipulating the interfacial layers at the metal-semiconductor interfaces. The manipulation of the interfacial layers modify the relative energy levels of the materials, which in turn either change the Schottky barrier height for cathode interface or enhance the ohmic contact for the anode interface.

The effect of the thin dielectric double layer on the rectifying cathode interface was studied by [21]. It was discovered that a thin organic or oxide interfacial barrier influences the properties of the copper-organic semiconductor contact. The double interfacial layer caused an increase in the energy barrier height. In addition, it was noted that the interfacial

layer might be capable of preventing hole injection into the semiconductor at reverse bias. However, the layer was thin enough to allow charge carrier movement under forward bias.

An ideal ohmic metal-semiconductor contact that does not add significant parasitic impedance to the device cannot be fabricated in reality, and a small contact resistance will normally be present in the fabricated diodes. A practical method for forming ohmic contacts is heavily doping the semiconductor in the contact region. Therefore, if a barrier exists at the interface, the depletion region is narrow enough to allow charge carriers to tunnel through the barrier. However, this method do not apply for organic semiconductors.

The practical method for p-type organic semiconductors is the use of a metal contact with higher work function compared with the HOMO level of the semiconductor. The HOMO levels of the organic semiconductors are approximately 5eV, but the available metals with work functions greater than 5eV are limited. Therefore, the utilization of different interfacial layers such as PEDOT:PSS [45], molybdenum oxide [46], and vanadium pentoxide [47] has been studied as a method to increase the effective electrode work functions. In addition, Lilja et al. proposed that a thin silver oxide layer on top of the printed silver enhances the ohmic contact of the anode interface [48], and the effect of the anodic silver oxides with different thicknesses on the performance of the organic Schottky diode was studied in [49]. In this thesis, the influence of the anodized silver oxide is further investigated.

3.3 Modeling and characterization

The analysis of the organic diode current density-voltage (JV) curves is the main method to characterize the rectification property of the diode. In fact, the quality of the diode contacts, rectification ratio, forward current characteristics and charge transport properties can be understood from the JV curves. However, the JV measurements only provide information about the DC properties of the diodes. Thus, the high frequency operation of the diode must be studied to obtain information about the AC behavior of the diode. In this section, the current-voltage characteristics and the high frequency operation of the printed organic Schottky diodes are discussed.

3.3.1 Current-voltage characteristics

As shown in Figure 3.9, the conduction of the MIM diode can be divided into three different regimes: reverse current region ($V < 0$), diffusion limited current region ($0 < V < V_d$) and space charge limited current (SCLC) region ($V > V_d$). In reverse biasing, the injection barrier for holes from the cathode to the HOMO of p-type semiconductors is high (Figure 3.9b). Therefore, the level of the resulting reverse leakage current is typically low. The latter two current regions are discussed as follows.

Injection and Diffusion limited current

As mentioned before, the ohmic contact between a metal and a fully depleted semiconductor can be described as an injecting contact, where the metal injects charges into the insulating material. When the voltage is below (V_d), the gradient of the hole density arises the diffusion of the holes towards the cathode (Figure 3.9c), resulting in the injection and diffusion limited current. On the other hand, the hole drift current due to the electric field is negative pointing toward the anode. However, the net current is dominated by the diffusion current, leading to a positive current from the anode to the cathode.

The diffusion limited current can be calculated by utilizing the familiar Shockley diode equation; however, this equation is derived to describe a bipolar current through a p-n junction. Thus, Applying this equation to unipolar devices with undoped semiconductors such as organic MIM diodes is questionable. In 2013, Bruynt et al. expressed the below equation for the hole-only diffusion in the MIM type devices:

$$J_{diff} = \frac{q\mu N_v \left(\phi_B - b - V\right)\left(e^{\frac{qV}{kT}} - 1\right)}{Le^{\frac{qb}{kT}}\left[e^{\frac{q(\phi_B - b)}{kT}} - e^{\frac{qV}{kT}}\right]}, \tag{3.3}$$

where N_v is the charge-carrier density at the ohmic contact interface, ϕ_B is the barrier height at the rectifying contact, b is the band bending parameter, and L is the thickness of the semiconductor [50]. The derivation was based on the modification of the classical diffusion theory of Schottky to consider an ideal ohmic contact, an undoped semiconductor and the absence of the band bending at the interfaces. The equation 3.3 is almost proportional to V, that is $J_{diff} \propto V$ as Figure 3.10 shows.

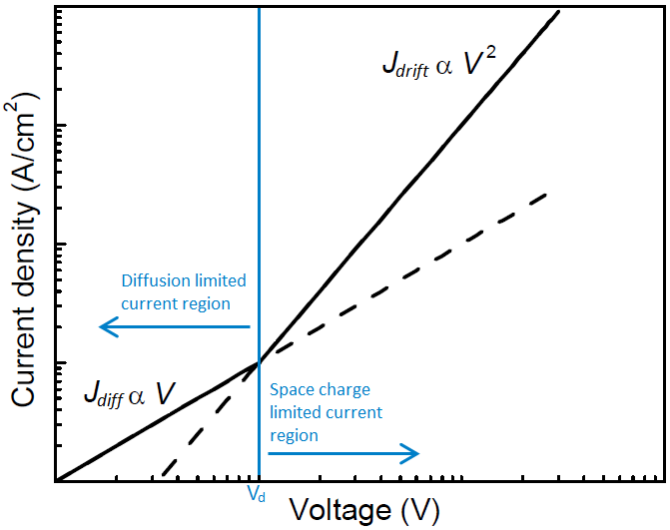

Figure 3.10 *Log-log plot of an ideal JV characteristic at forward biasing for an organic diode ([?], modified).*

Space charge limited current

Once enough charge has been injected into the semiconductor, the diode current is limited by the injected space-charge, and the JV characteristics of the diode follows the space charge limited current-theory, originally presented by Mott and Gurney in 1940 [51, 52].

When the density of the injected charge carriers increases so that their induced field dominates the filed due to the external applied biasing, the current is limited by the injected uncompensated space charges. This happens for voltages higher than V_d (Figure 3.9c). The SCLC follows the Mott-Gurney law:

$$J_{drift} = \frac{9\epsilon_r\epsilon_0 \left(V - V_{bi}\right)^2}{8L^3}, \tag{3.4}$$

where the semiconductor is assumed to be trap-free with a mobility independent of the electric field [52]. As described in equation 3.4, the SCLC is proportional to the square of the applied voltage ($J_{drift} \propto V^2$). This proportionality has been illustrated in Figure 3.10.

The derivation of the Mott-Gurney law uses three assumptions [52] which do not apply for organic semiconductors, namely that the device is trap-free, that diffusion is negligible and that the electric field at the injecting contact is zero. These assumptions are generally not correct, especially the assumption of trap-free organic semiconductors. In fact, the organic semiconducting materials usually have trap states within the band gap due to the charged defects [53]. Charged defects lead to barriers impeding the flow of the charge carriers and therefore lead to a reduced current. The reduced current results in an underestimation of the drift mobility and the level of the SCLC. Thus, in this case, the JV characteristics fit to a $J_{drift} \propto V^m$ law instead of a square law where m>2.

3.3.2 High frequency operation

Since the main application of organic Schottky diodes is in the high frequency rectifying circuits, it is essential to characterize the AC behavior of the diodes besides their DC characteristics. The high frequency operation of the diodes depends on the semiconductor properties, metal semiconductor interfaces and geometric parasitic impedances. The diode maximum operation frequency (f_{max}) is calculated based on the time that is required for the charge carriers to move from one electrode to the other, which is called the transit time (t_T). It is presented as:

$$f_{max} = \frac{1}{t_T} = \frac{\mu \left(V_{IN} - V_{DC}\right)}{L^2}, \tag{3.5}$$

where the V_{IN} is the input voltage, the V_{DC} is the DC output voltage, and L is the thickness of the semiconductor. However, the calculated f_{max} is overestimated since it assumes the optimal operation for the organic diodes.

In addition to the semiconductor bulk properties, the electrode interfaces also affect the AC characteristics of the diode. For instance, the interfacial trap states might decrease the injection velocity of the charge carriers, and thus the frequency operation of the diode.

The other important factor in the high frequency operation of the diode is the geometric parasitic impedances. The nature of the vertical sandwiched structure of the the organic Schottky diode results in a relatively high amount of parasitic geometric capacitance, which are obtained from:

$$C = \frac{\epsilon_r \epsilon_0 A}{L}, \tag{3.6}$$

where A is the cross-sectional area of the diode, L is the thickness of the semiconductor layer. The permittivity of the semiconductor (ϵ_r) is 3 For the PTAA semiconductor used in this work [49]. As a result, the simplest equivalent circuit for the the Schottky diode consists of a parallel connection of a resistor and a capacitor representing the bulk resistance and geometric capacitance of the diode, respectively. Since the depletion width of the organic MIM diodes do not change significantly with biasing voltage and the semiconductor is fully depleted, the capacitance of the diode remains practically constant over the useful biasing range.

3.4 Rectifiers

The rectifying circuits convert an input AC signal to an output DC voltage. High frequency (HF) rectification is needed especially in passive wireless applications. In fact, the needed power for the passive wireless devices is supplied by the AC signal harvested by the antenna. Therefore, the conventional RFID frequencies are interesting for the rectifying circuits. In other words, organic Schottky diodes can be used in RFID tags to convert the AC voltage captured by the antenna from a radio frequency (RF)-field to a DC voltage for the chip to use. In this thesis, the operation of the rectifying circuits is focused on the frequency of 13.56 MHz.

the performance of the printed organic diodes still does not meet standards of conventional electronic circuits, which limits their functionality and applicability. However, simple electronic circuits can be utilized. The simplest rectifier circuit is a half-wave rectifier consisting of a diode in series with a parallel RC load. Figure 3.11 illustrates a typical half-wave rectifier.

During the positive half-cycle of the incoming zero-to-peak AC voltage V_{IN}, the diode conducts and supplies power to the RC load, which charges the capacitor. During the negative half-cycle, the load resistor discharges capacitor. Thus, the overall output DC voltage V_{DC} remains almost constant with minimal ripples. The low forward voltage drop and minimum leakage current results in high V_{DC}. Also, the fast switching speed of the diode increases the performance of the rectifying circuit.

As mentioned before, the rectifying organic Schottky diodes are required to function reliably at the RFID frequency bands. However, the polymeric semiconductors possess intrinsically low charge carrier mobility, which impose limitations on the performance of the printed organic diodes. Thus, crystalline organic semiconductors are mostly utilized for high frequency rectification, which are almost vacuum processed [54,55] On the other hands, high rectifying printed diodes which can be fabricated under ambient conditions are highly demanded in printed electronics.

In addition to the half-way rectifier, It has been reported to exploit other rectifying circuits such as double half-way [56], full-way [57] and charge pump rectifying circuits [58] using organic diodes. In this thesis, the half-way rectifying circuits have been utilized as a measurement setup to evaluate the performance of the organic Schottky diode fabricated using reel-to-reel compatible printing processes and air stable amorphous p-type PTAA semiconductor.

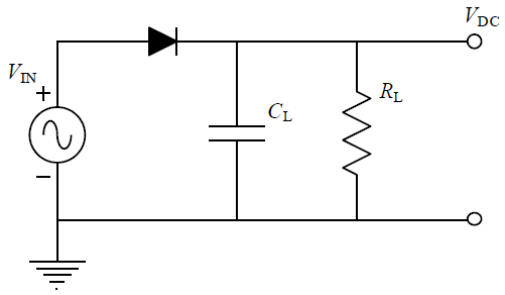

Figure 3.11 *Half-wave rectifier circuit. V_{IN} is the incoming AC signal, C_L is the load capacitance, R_L is the load resistance, and V_{DC} is the output DC voltage [21].*

4. OPTIMIZED OHMIC-CONTACT ORGANIC SCHOTTKY DIODE

In this chapter, a electrochemical anodic oxidation method to enhance the ohmic contact between the silver electrode and PTAA is studied. Three different thicknesses of anodic oxides are used in the study. The JV characteristics of the diodes are analyzed to see the effects of the thicknesses on the rectification ratio, forward and reverse currents. Also, the rectification property of the diodes are investigated in a half-way rectifying circuit. It is observed that the output DC voltage of the rectifier increases as a direct function of the oxide thicknesses. Thus, this method demonstrates the capability to effectively optimise the printed organic Schottky diodes.

4.1 Introduction

The performance of the printed MIM diodes with thin semiconductor layers depends on the charge injection and collection properties of the electrodes. A feasibly good ohmic contact provides maximum charge injection through the device with minimum contact resistances. Thus, formation of a good ohmic contact between the metal electrode and the semiconductor is essential.

One practical way to form practically good ohmic contacts is the utilization of heavily doped semiconductors right at the interface so that the depletion region is narrow enough for charge carriers to tunnel through the interface. However, this method is hardly applicable for organic semiconductors. In fact, the feasible method for organic semiconductors is the use of metals with appropriate work functions. The p-type semiconductor materials are more commonly used in printed electronics than the n-type materials due to higher air stability. However, The HOMO levels of the p-type organic semiconductors are near to 5eV, which restricts the applicable metals.

In the literature, the use of interfacial layers such as of PEDOT:PSS [45], molybdenum oxide [46], and vanadium pentoxide [47] at the ohmic interface has been reported. Nevertheless, deposition of ultra-thin additional layers complicates the fabrication process and limits the production volume. In 2003, Chen et al. showed enhanced hole injection in OLEDs using a thin oxide layer on top of the silver electrode [59]. In 2010, Lilja et al. proposed that a thin oxide layer on top of the printed silver electrode improves the ohmic contact with PTAA semiconductor [48]. The influences of the silver anodic oxides on the performance of the diodes was reported in [49]. In this thesis, the optimization of

the ohmic contact using anodic oxidation method to form anodic silver oxide layers with different thicknesses is further studied.

4.2 Experimental section

The diodes are manufactured in a dust-free environment (noncertified but close to ISO 14644-1 class 5) at room temperature and relative humidity of 40-50%. The fabrication process is described in section 4.2.1 and 4.2.2. Fourteen samples per each diode structure are fabricated and measured. All measurements are performed in ambient laboratory conditions. The measurement equipment and methods are presented in section 4.2.3.

4.2.1 Preparation steps

The sample preparation process is depicted in Figure 4.1. The PET substrates (Melinex ST506, from Dupont Teijin Films [20]) are cleaned with 2-propanol solution (IPA) and deionized water (DI-water). After cleaning, silver bottom electrode with the thickness of 100nm is e-beam vacuum evaporated on the substrate (2Å/s, 10^{-7}mbar) (Figure 4.1a). The native oxide on top of the evaporated silver cannot be avoided due to the ambient processing conditions [60].

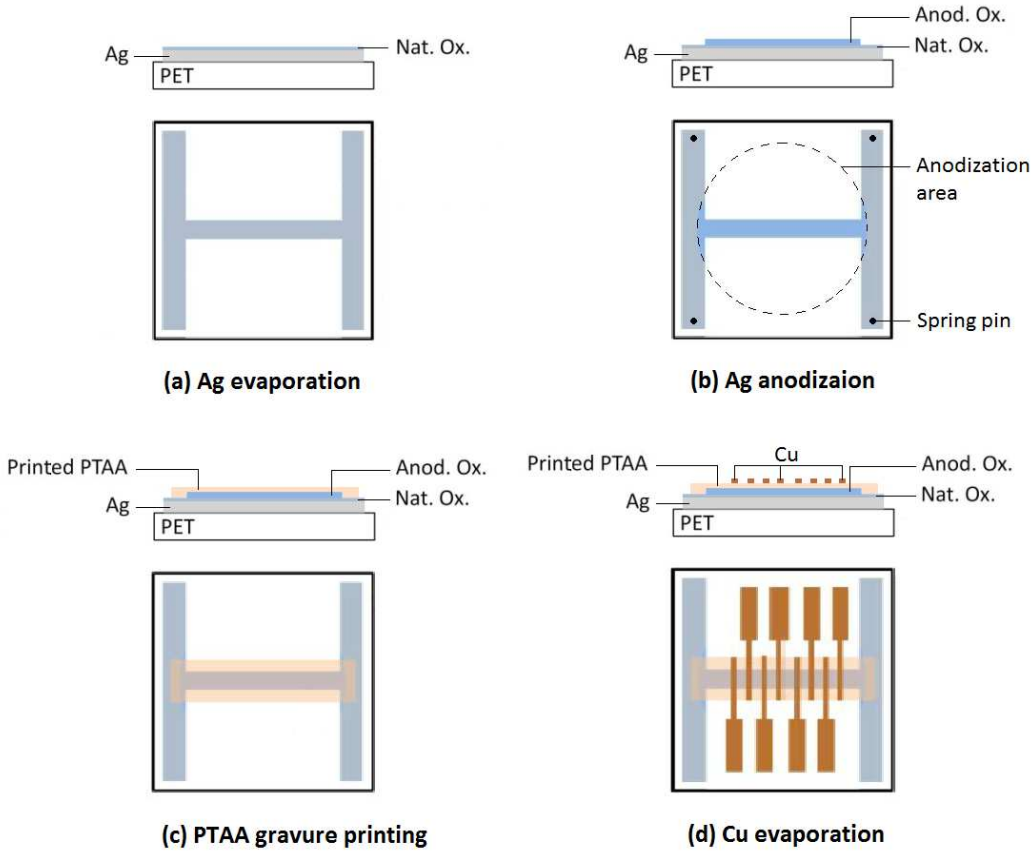

Figure 4.1 *Sample preparation process: (a) silver evaporation, (b) silver anodization, (c) PTAA gravure printing, and (d) copper evaporation (modified [49]).*

Immediately after evaporation, anodic oxidation of the evaporated silver is performed in stirred 0.5M NaOH electrolyte at room temperature (Figure 4.1b). The anodization is done with Zennium electrochemical workstation from Zahner Elektrik GmbH [61]. The anodization process is introduced in section 4.2.2. After anodization, the samples are cleaned with IPA.

The PTAA semiconductor is gravure printed on top of the anodic oxidized silver electrode (Figure 4.1c) using a laboratory-scale gravure printing press, Labratester Automatic from Norbert Schäfli Maschinen [62]. The PTAA is cured at 60°C for 5 min. Finally, top electrodes of copper with the thicknesses of 100nm are evaporated through shadow masking (Figure 4.1d).

All processing steps, except electrodes evaporation, are performed in ambient air conditions.

4.2.2 Anodization

Anodization is an electrolytic passivation process utilizing the modern electrolysis methods to make the target metal passive so that it is less affected by environmental factors such as air and water. The process is called anodizing because the treated metal forms the anode electrode of an electrolytic cell. The anodization is a large area high-throughput process usually used to strengthen and preserve the appearance of metallics by develops a light anodic film of metal oxide to shield and protect the base material against corrosion. However, it can be used to increase the thickness of the oxide layer on the surface of metal parts. The anodized layer thicknesses can be calculated based on *Faraday's law*.

Anodic oxides differ from natural oxides due to the porosity that the anodic process imposes on the surface texture. thick anodic coatings are normally more porous. The porosity augments the hydrophilicity of the surface, and provides more adherent surfaces. Thus, the adhesion of the PTAA on the silver surface increases resulting in thinner and more uniform semiconductor layers with less holes and defects. Holes and defects can reduce the amount of the working diodes by making short circuit paths.

Before discussing the silver anodization, it is beneficial to introduce the modern electrolysis method and Faraday's laws of electrolysis.

modern electrolysis

modern electrolysis method involves a system consisting of three electrodes: working electrode, reference electrode and auxiliary (or counter) electrode. The reference electrode has been added in order to provide a reference constant potential, while the counter electrode supplies the electrons needed to counter redox events at the working electrode. This extra reference electrode is required since it is difficult for a single electrode to maintain a constant potential while passing current.

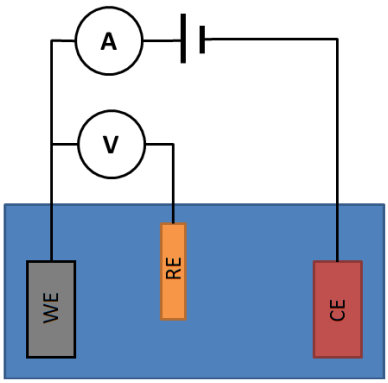

Figure 4.2 *Three electrode system consisting of Working Electrode (WE), Reference Electrode (RE) and Counter Electrode (CE) (modified [63]).*

Actually, the roles of supplying electrons and providing a reference potential are divided between two separate electrodes: counter and reference electrodes. The counter electrode is fabricated from electrochemically inert materials with good conductivities such as gold [64], platinum, or carbon [65] so that it has no chemical reaction with the electrolyte and passes the current with minimum resistance. The reference electrode is a half cell with a known reduction potential. It acts as the reference in measuring and controlling the potential of the working electrode, and it passes no current. The counter electrode passes all the current needed at the working electrode.

Faraday's laws of electrolysis

Faraday studied the relationship between the amount of a substance deposited or dissolved during the electrolysis of aqueous solutions and the quantity of electricity passed through the electrolyte. He established it in the form of two laws of electrolysis.

- **Faraday's first law of electrolysis**: the amount of a substance deposited or dissolved as a result of passage of an electric current is directly proportional to the quantity of electricity passed or

$$m = eQ, \tag{4.1}$$

  where m[g] is the mass of the substance deposited or dissolved, Q[C] is the quantity of electrical charge, and e is a constant called the *electrochemical equivalent* (ECE). For one coulomb of electricity, the weight of the substance deposited or dissolved equals to ECE.

- **Faraday's second law of electrolysis**: for the same quantity of electricity passed through different electrolytes, the amounts of different substances deposited or dissolved are proportional to their chemical equivalent weights or

$$\frac{m_1}{m_2} = \frac{E_1}{E_2} = \frac{e_1}{e_2}, \tag{4.2}$$

where E[g] is the chemical equivalent weight. The quantity of electricity required to deposit or dissolve one gram of E is equal to F coulombs ($F = E/e$). F is called *faraday* whose value equals to 96,450 coulombs.

Combining the two laws:

$$m = Q\left(\frac{E}{F}\right), \tag{4.3}$$

or by substituting E with (M/z)

$$m = \left(\frac{Q}{F}\right)\left(\frac{M}{z}\right), \tag{4.4}$$

where M[g/mol] is the molar mass, and z is the number of change in the oxidation state under electrolysis.

When more than one process occurs at the electrodes, the amounts deposited or dissolved in all the processes have to be considered. For instance, when zinc or nickel solutions are electrolysed, two processes occur at the cathode, which are the deposition of the metal and the evolution of hydrogen [66]. In such cases the term *current efficiency* (n) is defined to indicate the extent of the primary electrode reaction. It is the ratio of the actual amount of the material deposited or dissolved and that theoretically expected to be deposited or dissolved based on Faraday's laws. Thus, equation 4.5 can be modified as

$$m = n\left(\frac{Q}{F}\right)\left(\frac{M}{z}\right). \tag{4.5}$$

Silver anodization

Evaporated films of silver are anodically oxidized in 0.5M NaOH buffer solutions at room temperature. The samples are mounted in a sample holder fabricated of polyether ether ketone (PEEK). The front side of the sample holder contains a platinum mesh (25cm^2) as the counter electrode, which is fixed at a distance of 18mm from a place provided for the working electrode. The square-shape PET samples, on which the silver film is evaporated, fix in the provided position such that all four spring pins are in contact with the silver film (Figure 4.1b). All these spring pins were short circuited to form the electrical contact for the working electrode. The anodization area exposed to the electroclyte is 2.4 cm^2, but the anodized silver area is only 0.32cm^2.

An Ag/AgCl reference electrode (in 3M KCl with constant potential of +0.27V) is located amid the counter and working electrodes as close to the working electrode as possible. The electrolyte is continuously stirred during the anodization. A Zennium electrochemical workstation (Zahner Elektrik GmbH) is utilized to perform the anodization and the analysis of the measured data. Uncompensated resistances, arouse from the electrolyte and wiring, are negligible compared to the actual oxide layer resistance.

The anodic oxidation of silver in aqueous alkaline electrolytes is a complex process involving a number of reaction steps and phase formation phenomena. The silver/silver-oxide system has been intensively studied in the past (look at [67] for references) not only due to its use in batteries but also as a model to investigate the mechanism of the electrochemically surface oxide formation. Potentiodynamic, potentiostatic and galvanostatic studies of this electrode system reveals that the overall oxidation process involves a successive formation of Ag_2O and AgO according to the reactions [68]:

$$2\,Ag + 2\,OH^- \longleftrightarrow Ag_2O + H_2O + 2\,e^- \tag{4.6}$$

$$Ag_2O + 2\,OH^- \longleftrightarrow 2\,AgO + H_2O + 2\,e^- \tag{4.7}$$

The AgO layer is formed at more anodic potentials on top of the Ag_2O film. The anodic Ag_2O film consists of a homogeneous, but hydrous, primary oxide layer with a disordered structure on which a secondary more porous layer nucleates exhibiting the crystalline structure of Ag_2O. In this work, the initial stages of the anodic silver oxidation is assumed to exist due to the low anodization potential. Thus, a monolayer of Ag_2O is presumably developed on the silver surface. This monolayer grows to form a thicker multilayer with increasing the anodization potential.

The thickness of the anodized oxide layer (Δd_{ox}[cm]) can be calculated using the Faraday's law (equation 4.5) by substituting m by $\rho_{ox} A d_{ox}$, where ρ_{ox}[g/cm^3] is the volume density of the oxide, A[cm] is the area of the anodic oxide. Then

$$\Delta d_{ox} = n\Big(\frac{M_{ox}}{A\rho_{ox} z F}\Big)\Delta Q, \tag{4.8}$$

where M_{ox}[g/mol] is the molar mass of the oxide. In the case of the silver oxide product (Ag_2O), z equals to 1, M_{ox} equals to 231.735[g/mol] and ρ_{ox} equals to 7.14[g/cm^3]. The efficiency factor (n) is assumed 1 due to the lack of oxygen evolution for low anodization potentials. As mentioned before, the anodic oxide area on the sample is 0.32cm^2.

In this thesis, the anodization process is performed galvanostatically, which means that the anodization current is kept constant during anodization. Thus, integrating the anodization current over time, the transferred charge ΔQ is equal to $I\Delta t$, where I[A] is the anodizing current and t[s] is the anodizing time. Rearranging equation 4.8, the required anodizing times corresponding to the desired anodic oxide thicknesses can be obtained from

$$\Delta t = \Big(\frac{d_{ox}\rho_{ox} A}{M_{ox}}\Big)\Big(\frac{F}{I}\Big), \tag{4.9}$$

where z and n are substituted by 1.

Three different thicknesses (2nm, 4nm and 6nm) of the Ag_2O are anodized so that it is possible to study the oxide influence on the device operation. The corresponding required times are obtained from equation 4.9 (4.75s, 9.5s and 14.3s, respectively for I=40μA). The anodization currents and potentials during the anodic oxidation process are presented in Figure 4.3.

The galvanostatic anodization process is divided into three phases. During the first phase, the open circuit potential is measured for 60s (I=0), while the electrolytic system stabilizes. this system stabilization improves the reproducibility of the experiment. The second phase launches the actual anodization process, where a constant current is passed through the WE. In the third phase, the open circuit potential is measured again as long as the whole measurement time is 120s. The last phase at the end of the process demonstrated a clear change in the sample potential. Thus, it can be deducted that the process clearly change the properties of the sample surface.

4.2.3 Measurements

Referring to Figure 4.2, the last step in the diode fabrication process was the copper evaporation. The samples are kept in the vacuum evaporation chamber overnight before measurement. Diode JV and AC rectification characteristics were measured. The measurement setup was implemented during the previous thesis work presented in [69]. A LabVIEW® computer interface and a standard half-wave rectifying circuit along with the calibration kit for the capacitance measurement were made.

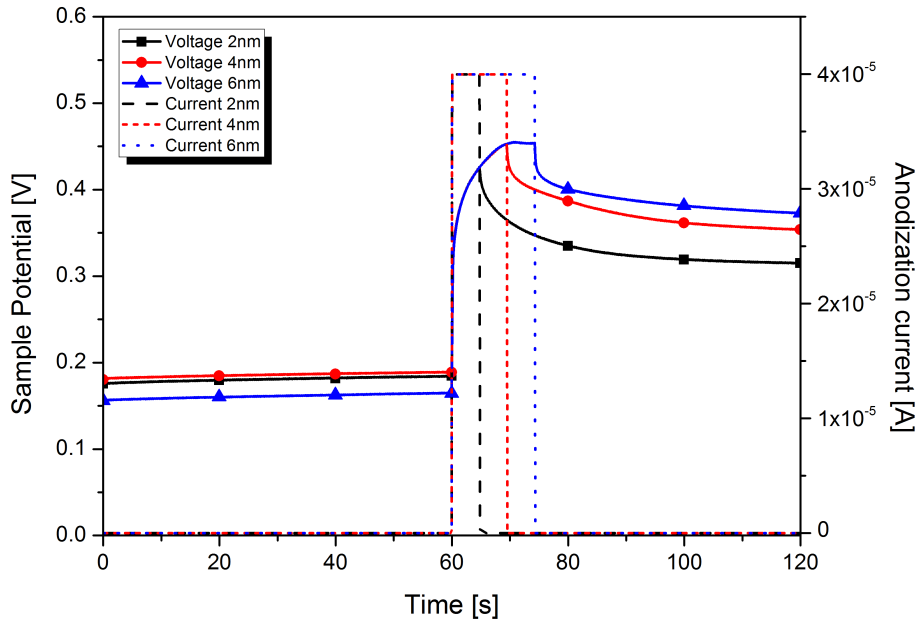

Figure 4.3 *Anodization currents and sample potentials during the anodic oxidation of silver.*

The half-wave rectifier is made of 47nF load capacitor. a input signal with the peak-to-peak voltage of 10V AC is used in the AC rectification measurement, and the internal resistance of the oscilloscope, which is 1MΩ, is considered as the output load of the rectifier. More discussion of the JV and the AC rectification characteristics is presented in section 4.3.

The JV characteristics are measured using the Keithley 236 source-measure unit, and the AC rectification measurement is done using the LabVIEW® computer interface.

The geometric capacitance is measured to estimate the diode thickness of different samples. The diode thicknesses present the resemblance of separate samples. The capacitance measurement is done using *hp*® Network analyzer 8752A. Using the relative permittivity of the semiconductor (ϵ_r=3) and the diode active area (1mm^2), the measured capacitance value of 50pF translates into a thickness of 530nm.

4.3 Results and discussion

The performance of the fabricated organic Schottky diodes is evaluated based on the measured JV and AC (alternating current) rectification curves of the diodes. The JV and the AC rectification curves are evaluated based on the models presented in section 3.2 and 3.3. JV curves illustrates that the anodic silver oxide enhances the charge carrier injection, thereby increasing the rectification ratio. It is expected that the increase in the rectification ratio increases the DC output of the AC rectification curves. Although, the presence of the trap states in the semiconductor can change the level of the DC output. The results and the discussion are presented in the subsequent sections.

4.3.1 JV curves

The JV curves of the diodes can depict how the quality of the contacts at the anode and the cathode interfaces affect the performance of the diodes. The forward current can indicate the level of the Schottky barrier at the copper-PTAA interface, and the level of the forward current can illustrate the the injection level at the silver-PTAA interface. A good ohmic contact at the silver-PTAA interface can guarantee the maximum injection of the holes from the silver contact. The measured JV curves for diodes with three different anodic oxide thicknesses (2nm, 4nm and 6nm) are shown in Figure 4.4. The curves shown in Figure 4.4 are the mean values of the JV curves measured for different prototypes along with the error bars representing the standard deviation for some selected data points.

Figure 4.4 shows that the reverse currents are relatively constant for different thicknesses of the anodic oxides. The consistency of the reverse currents is due to the formation of a constant Schottky barrier at the copper-PTAA interface because of the Fermi energy levels, as mentioned in section 3.2. This constant Schottky barrier leads to a constant diffusion potential which imposes the consistency of the reverse currents.

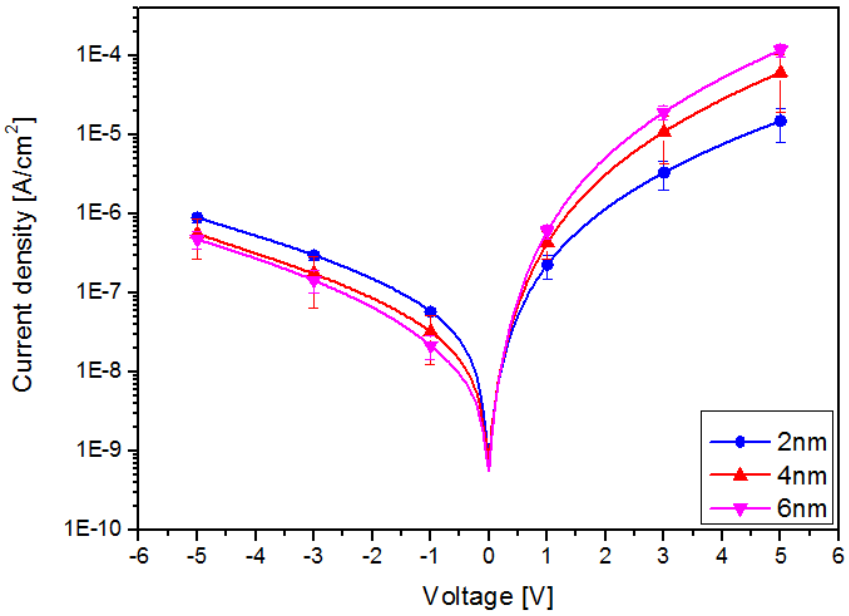

Figure 4.4 *JV curves of organic Schottky diodes for different thicknesses of the silver anodic oxides. The error bars represents the standard deviation of the working samples.*

On the other hand, the level of the forward current increases as the thickness of the anodic oxide increases. This can be due to the fact that the level of the hole injections increases for thicker oxide layers, while it can be assumed that the work function of the silver is quite constant for different thicknesses of anodic oxides. As mentioned before, the work function of the metal determines the quality of the ohmic contact, which in turn limits the injection of the charge carriers from the silver contact. While the quite same surface structures of different anodic oxides result in quite same work functions, the injection barrier of the ohmic contacts can be assumed similar. Thus, the level of the forward current increases not because of different work functions, but because of increasing hole injections that thicker anodic oxides make.

A more thorough evaluation of the forward current can be done with utilizing a full logarithmic representation. Figure 4.5 shows the full logarithmic representation of the forward currents for the same curves of Figure 4.4b. As shown in this graph, the current has an ohmic dependence on voltage ($J \propto V^{0.9}$) for lower voltages, whereas it is almost cubicly proportional to the voltage ($J \propto V^{2.7}$) for higher voltages. This graph is compatible with the model presented in section 3.3. As mentioned in that section, the presence of the trap states due to the charged defects throughout the semiconductor leads to a barrier near the ohmic contact which impedes against the flow of the holes in the same way as the diffusion potential does [53]. In fact, the SCLC happens for the higher voltages when this barrier is reduced.

These trap states also influence the performance of the rectification as presented in next section.

4.3.2 AC rectification curves

From Figure 4.4b, it can be understood that the rectification ratio increases with the increase of the anodic oxide thickness. The rectification ratio is defined as the ratio of the currents for the voltages of +5V and -5V. It is expected to obtain higher DC output voltages for higher values of this ratio. The mean values of the DC output levels for a half-wave rectifying circuit is illustrated in Figure 4.6 both for native and anodic oxides. As shown in this graph, the DC output level for the native oxide is less than those of the anodic oxides due to its lower rectification ratio. The DC output level is increasing with the increase of the anodic oxide thickness. However, as the error bars show, the standard deviation factors are large resulted from the significant discrepancies between the DC output levels of different prototypes with the same thickness of the anodic oxide. Also, the quality of the contact imposes an injection barrier, which in turn reduce the current level for the same voltages.

In fact, different DC output levels obtained for different diodes with the same anodic oxide thickness, while their rectification ratios were near to each other. This can be due the presence of the trap states within the semiconductor. Actually, these trap states trap the injected holes in the first positive half-cycle of the incoming signal. These trapped holes do not completely depleted during the next negative half-cycle. On the other hand, the the density of the charged defects can be different for different prototypes, thus changing the level of the depleted holes. This fact results in different current level, and in turn, leading to different DC output levels.

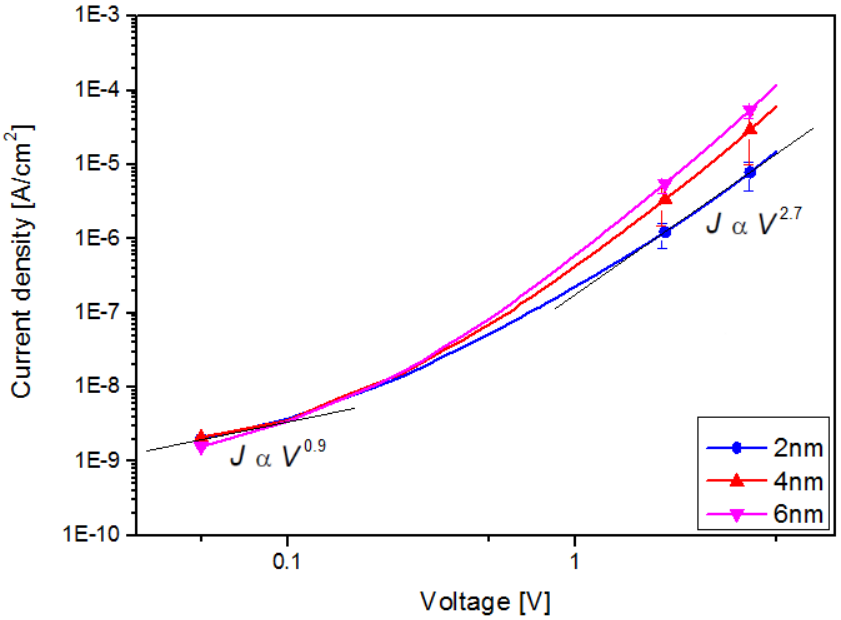

Figure 4.5 *Log-Log JV characteristics for organic Schottky diodes with different thicknesses of anodic oxides.*

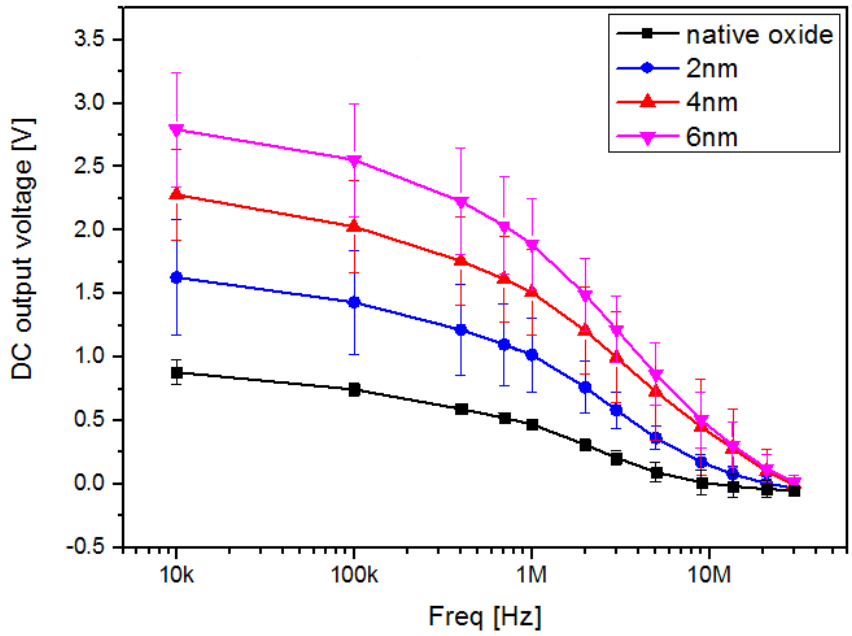

Figure 4.6 *AC rectification characteristics of organic Schottky diodes with native oxide and different thicknesses of anodic oxides.*

4.4 Conclusion

In this section, the effect of the anodic oxide and the anodization process on the performance of the fabricated organic Schottky diodes have been investigated through evaluation of their JV and AC rectification curves. As discussed before, the increasing thicknesses of the anodic oxide increase the rectification ratios, thus increasing the output DC levels of the half-wave rectifying circuit. The performance of the diodes was evaluated based on the models presented in section 3.2 and 3.3.

5. CONCLUSIONS

In this thesis, the organic Schottky diodes with different thicknesses of the silver oxides were fabricated. The silver oxides were made utilizing anodization process, which is an electrochemical process to treat the surface of the silver contact. That way, the performance of the diodes were optimized through controlling the thickness of the silver oxdie at the ohmic interface of the organic Schottky diodes. This optimization leaded to more injection of holes from the silver contact to the semiconductor, which increased the diode forward current by 1 order of magnitude and, thus, the rectification ratio. The increase of the rectification ratio increased the DC output of the half-wave rectifying circuit. The DC output was varying for different diodes with the same thickness of the anodic oxide because the holes might trap in the charged states throughout the semiconductor layer. However, the overall DC output of the diodes increased for thicker anodic oxide layers. the printing process.

The auspicious results of this thesis opened the path for further research on optimizing the performance of the printed organic Schottky diodes. The optimized diodes showed the capability to have the desirable properties, which are high rectifications ratio, high forward current and high DC output of the rectifying circuit. Future research can concentrate on improving the properties of the diodes through examining the diodes with thicker anodic oxide layers, improving the printing processes or enhancing the treatment of the semiconductor layers to decrease the density of the charged defects.

REFERENCES

[1] B.G. Streetman and S. Banerjee. *Solid state electronic devices*. Prentice-Hall Upper Saddle River, NJ, 6th edition, 2006.

[2] Y. Sun, Y. Liu, and D. Zhu. Advances in organic field-effect transistors. *Journal of materials Chemistry*, 15(1):53–65, 2005.

[3] G. Strobl. *The physics of polymers*. Springer, 3rd edition, 2006.

[4] H. Shirakawa, E.J. Louis, A.G. MacDiarmid, C.K. Chiang, and A.J. Heeger. Synthesis of electrically conducting organic polymers: halogen derivatives of polyacetylene, $(CH)_x$. *J. Chem. Soc., Chem. Commun.*, (16):578–580, 1977.

[5] A.J. Heeger, A.G. MacDiarmid, and H. Shirakawa. The Nobel Prize in chemistry, 2000: conductive polymers. *Stockholm, Sweden: Royal Swedish Academy of Sciences*, 2000.

[6] J.H. Burroughes, D.D.C Bradley, A.R. Brown, R.N. Marks, K. Mackay, R.H. Friend, P.L. Burns, and A.B. Holmes. Light-emitting diodes based on conjugated polymers. *nature*, 347(6293):539–541, 1990.

[7] S. Günes, H. Neugebauer, and N.S. Sariciftci. Conjugated polymer-based organic solar cells. *Chemical reviews*, 107(4):1324–1338, 2007.

[8] Z. Bao and J. Locklin. *Organic field-effect transistors*. CRC press, 2007.

[9] I. Kymissis. *Organic Field Effect Transistors: Theory, Fabrication and Characterization*. Springer, 2008.

[10] V. Rani and K.S.V. Santhanam. Polycarbazole-based electrochemical transistor. *Journal of Solid State Electrochemistry*, 2(2):99–101, 1998.

[11] J.T. Mabeck and G.G. Malliaras. Chemical and biological sensors based on organic thin-film transistors. *Analytical and bioanalytical chemistry*, 384(2):343–353, 2006.

[12] S.M. Goetz, C.M. Erlen, H. Grothe, B. Wolf, P. Lugli, and G. Scarpa. Organic field-effect transistors for biosensing applications. *Organic Electronics*, 10(4):573–580, 2009.

[13] H. Frauenrath. Organic electronic materials - synthesis, properties, applications. http://lmom.epfl.ch/index.php?page=organicelectronics, 2014. École polytechnique fédérale de Lausanne.

[14] H.A.M. Van Mullekom, J.A.J.M. Vekemans, E.E. Havinga, and E.W. Meijer. Developments in the chemistry and band gap engineering of donor–acceptor substituted conjugated polymers. *Materials Science and Engineering: R: Reports*, 32(1):1–40, 2001.

[15] B.S. Hudson and D.G. Allis. Bond alternation in infinite periodic polyacetylene: Dynamical treatment of the anharmonic potential. *Journal of Molecular Structure*, 1032:78–82, 2013.

[16] J. Hwang, D.B. Tanner, I. Schwendeman, and J.R. Reynolds. Optical properties of nondegenerate ground-state polymers: Three dioxythiophene-based conjugated polymers. *Physical Review B*, 67(11):115205, 2003.

[17] C. Anderson and E. Davidson. Conducting polymers. http://budker.berkeley.edu/Physics141_2013/AndersonDavidson%20-%20Conducting%20Polymers%204-25-2013.pdf, 2013. University of California, Berkeley.

[18] T. Oyamada, H. Uchiuzou, S. Akiyama, Y. Oku, N. Shimoji, K. Matsushige, H. Sasabe, and C. Adachi. Lateral organic light-emitting diode with field-effect transistor characteristics. *Journal of applied physics*, 98(7):074506, 2005.

[19] S. Mutlu, I. Haydaroglu, and A.O. Sevim. Realization of polymer charge pump circuits using polymer semiconductors. *Organic Electronics*, 12(2):312–321, 2011.

[20] Melinex st506/505 film. http://inkjetflex.com/site/wp-content/uploads/2009/09/Melinex_ST505.pdf, 2009. DuPondTeijinFilms.

[21] K. Lilja. Performance, interfacial properties and applications of printed organic diodes. *Tampereen teknillinen yliopisto. Julkaisu-Tampere University of Technology. Publication; 1006*, 2011.

[22] J. Veres, S. Ogier, S. Leeming, B. Brown, and D. Cupertino. Air stable, amorphous organic films and their applications to solution processable flexible electronics. In *Materials Research Society Symposium Proceedings*, volume 708, pages 243–250. Warrendale, Pa.; Materials Research Society; 1999, 2002.

[23] K. Lilja, T.G. Bäcklund, D. Lupo, J. Virtanen, E. Hämäläinen, and T. Joutsenoja. Printed organic diode backplane for matrix addressing an electrophoretic display. *Thin Solid Films*, 518(15):4385–4389, 2010.

[24] T. Kawase, T. Shimoda, C. Newsome, H. Sirringhaus, and R.H. Friend. Inkjet printing of polymer thin film transistors. *Thin Solid Films*, 438:279–287, 2003.

[25] A.M. Nardes, M. Kemerink, M.M. De Kok, E. Vinken, K. Maturová, and R.A.J. Janssen. Conductivity, work function, and environmental stability of PEDOT:PSS thin films treated with sorbitol. *Organic Electronics*, 9(5):727–734, 2008.

[26] A. Vollmer, H. Weiss, S. Rentenberger, I. Salzmann, J.P. Rabe, and N. Koch. The interaction of oxygen and ozone with pentacene. *Surface science*, 600(18):4004–4007, 2006.

[27] P. Heljo. Organic diodes for high frequency and logic applications. *Tampereen teknillinen yliopisto. Julkaisu-Tampere University of Technology. Publication; 1264*, 2014.

[28] D.T. James, B.K.C. Kjellander, W.T.T. Smaal, G.H. Gelinck, C. Combe, I. McCulloch, R. Wilson, J.H. Burroughes, D.D.C. Bradley, and J.S. Kim. Thin-film morphology of inkjet-printed single-droplet organic transistors using polarized raman spectroscopy: effect of blending tips-pentacene with insulating polymer. *Acs Nano*, 5(12):9824–9835, 2011.

[29] D. Choi, B. Ahn, S.H. Kim, K. Hong, M. Ree, and C.E. Park. High-performance triisopropylsilylethynyl pentacene transistors via spin coating with a crystallization-assisting layer. *ACS applied materials & interfaces*, 4(1):117–122, 2011.

[30] P. Kopola, M. Tuomikoski, R. Suhonen, and A. Maaninen. Gravure printed organic light emitting diodes for lighting applications. *Thin Solid Films*, 517(19):5757–5762, 2009.

[31] P.H. Lau, K. Takei, C. Wang, Y. Ju, J. Kim, Z. Yu, T. Takahashi, G. Cho, and A. Javey. Fully printed, high performance carbon nanotube thin-film transistors on flexible substrates. *Nano letters*, 13(8):3864–3869, 2013.

[32] M.M. Voigt, R.C.I. Mackenzie, S.P. King, C.P. Yau, P. Atienzar, J. Dane, P.E. Keivanidis, I. Zadrazil, D.D.C. Bradley, and J. Nelson. Gravure printing inverted organic solar cells: The influence of ink properties on film quality and device performance. *Solar Energy Materials and Solar Cells*, 105:77–85, 2012.

[33] K.E. Lilja, T.G. Bäcklund, D. Lupo, T. Hassinen, and T. Joutsenoja. Gravure printed organic rectifying diodes operating at high frequencies. *Organic Electronics*, 10(5):1011–1014, 2009.

[34] F.C. Krebs, J. Fyenbo, and M. Jørgensen. Product integration of compact roll-to-roll processed polymer solar cell modules: methods and manufacture using flexographic printing, slot-die coating and rotary screen printing. *Journal of Materials Chemistry*, 20(41):8994–9001, 2010.

[35] D. Deganello, J.A. Cherry, D.T. Gethin, and T.C. Claypole. Patterning of micro-scale conductive networks using reel-to-reel flexographic printing. *Thin Solid Films*, 518(21):6113–6116, 2010.

[36] C.F. Huebner, J.B. Carroll, D.D. Evanoff, Y. Ying, B.J. Stevenson, J.R. Lawrence, J.M. Houchins, A.L. Foguth, J. Sperry, and S.H. Foulger. Electroluminescent colloidal inks for flexographic roll-to-roll printing. *Journal of Materials Chemistry*, 18(41):4942–4948, 2008.

[37] H.J. Lewis and A. Ryan. *New Trends in Technologies: Devices, Computer, Communication and Industrial Systems*, chapter 20, pages 375–402. Sciyo, 2010.

[38] B. Peng and P.K.L. Chan. Flexible organic transistors on standard printing paper and memory properties induced by floated gate electrode. *Organic Electronics*, 15(1):203–210, 2014.

[39] Y. Galagan, J.E.J.M. Rubingh, R. Andriessen, C.C. Fan, P.W.M. Blom, S.C. Veenstra, and J.M. Kroon. ITO-free flexible organic solar cells with printed current collecting grids. *Solar Energy Materials and Solar Cells*, 95(5):1339–1343, 2011.

[40] J. Virkki, T. Björninen, T. Kellomäki, S. Merilampi, I. Shafiq, L. Ukkonen, L. Sydänheimo, and Y.C. Chan. Reliability of washable wearable screen printed UHF RFID tags. *Microelectronics Reliability*, 54(4):840–846, 2014.

[41] V. Pynttari, E. Halonen, H. Sillanpaa, M. Mantysalo, and R. Makinen. RF design for inkjet technology: Antenna geometries and layer thickness optimization. *Antennas and Wireless Propagation Letters, IEEE*, 11:188–191, 2012.

[42] S.Y. Cho, J.M. Ko, J.Y. Jung, J.Y. Lee, D.H. Choi, and C. Lee. High-performance organic thin film transistors based on inkjet-printed polymer/TIPS pentacene blends. *Organic Electronics*, 13(8):1329–1339, 2012.

[43] M. Mengel and I. Nikitin. Inkjet printed dielectrics for electronic packaging of chip embedding modules. *Microelectronic Engineering*, 87(4):593–596, 2010.

[44] D. Braga, M. Campione, A. Borghesi, and G. Horowitz. Organic metal-semiconductor field-effect transistor (OMESFET) fabricated on a rubrene single crystal. *Advanced materials*, 22(3):424–428, 2010.

[45] J. Kwon, Y.G. Seol, N.E. Lee, and I. Chung. Study on ohmic contact improvement of organic Schottky diode utilizing self-assembled monolayer and PEDOT:PSS layers. *Journal of Vacuum Science & Technology A*, 28(4):879–885, 2010.

[46] Z. Lü, Z. Deng, J. Zheng, Y. Zou, Z. Chen, D. Xu, and Y. Wang. Ohmic contact and space-charge-limited current in molybdenum oxide modified devices. *Physica E: Low-dimensional Systems and Nanostructures*, 41(10):1806–1809, 2009.

[47] P. De Bruyn, D.J.D. Moet, and P.W.M. Blom. All-solution processed polymer light-emitting diodes with air stable metal-oxide electrodes. *Organic Electronics*, 13(6):1023–1030, 2012.

[48] K.E. Lilja, H.S. Majumdar, F.S. Pettersson, R. Osterbacka, and T. Joutsenoja. Enhanced performance of printed organic diodes using a thin interfacial barrier layer. *ACS applied materials & interfaces*, 3(1):7–10, 2010.

[49] P.S. Heljo, H.S. Majumdar, and D. Lupo. high throughput electrochemical method for ohmic contact optimization in printed rectifying contacts. In *MRS Proceedings*, volume 1628. Materials Research Society, 2014.

[50] P. De Bruyn, A.H.P. Van Rest, G.A.H. Wetzelaer, D.M. de Leeuw, and P.W.M. Blom. Diffusion-limited current in organic metal-insulator-metal diodes. *Physical review letters*, 111(18):186801, 2013.

[51] A. Rose. Space-charge-limited currents in solids. *Physical Review*, 97(6):1538, 1955.

[52] Ho-Kei Chan. *Ferroelectrics - Characterization and Modeling*, chapter 24, pages 467–490. InTech, 2011.

[53] T. Kirchartz. Influence of diffusion on space-charge-limited current measurements in organic semiconductors. *Beilstein journal of nanotechnology*, 4(1):180–188, 2013.

[54] R. Rotzoll, S. Mohapatra, V. Olariu, R. Wenz, M. Grigas, K. Dimmler, O. Shchekin, and A. Dodabalapur. Radio frequency rectifiers based on organic thin-film transistors. *Applied Physics Letters*, 88(12):123502–123502, 2006.

[55] S. Steudel, K. Myny, V. Arkhipov, C. Deibel, S. De Vusser, J. Genoe, and P. Heremans. 50 MHz rectifier based on an organic diode. *Nature materials*, 4(8):597–600, 2005.

[56] K. Myny, S. Steudel, P. Vicca, J. Genoe, and P. Heremans. An integrated double half-wave organic schottky diode rectifier on foil operating at 13.56 MHz. *Applied physics letters*, 93(9):093305, 2008.

[57] P.S. Heljo, M. Li, K.E. Lilja, H.S. Majumdar, and D. Lupo. Printed half-wave and full-wave rectifier circuits based on organic diodes. *Electron Devices, IEEE Transactions on*, 60(2):870–874, 2013.

[58] P. Heljo, K.E. Lilja, H.S. Majumdar, and D. Lupo. High rectifier output voltages with printed organic charge pump circuit. *Organic Electronics*, 15(1):306–310, 2014.

[59] C.W. Chen, P.Y. Hsieh, H.H. Chiang, C.L. Lin, H.M. Wu, and C.C. Wu. Top-emitting organic light-emitting devices using surface-modified Ag anode. *Applied physics letters*, 83(25):5127–5129, 2003.

[60] A. De Rooij. The oxidation of silver by atomic oxygen. *EsA Journal*, 13:363–382, 1989.

[61] Zahner Elektrik GmbH. Electrochemical workstation Zennium. http://www.zahner.de/products/electrochemistry/zennium.html, 2014. 2015-03-04.

[62] Norbert Schäfli Maschinen. Laboratory gravure printing machine. http://www.nsmz.com/index.php/en/products/laboratory-printing-machines/labratester, 2014. 2015-03-04.

[63] Univerzita Karlova Surface Physics Group. Cycling voltammetry: principle. http://physics.mff.cuni.cz/kfpp/povrchy/method/cv-principles. 2015-03-13.

[64] S.N. Lvov, S.R. Narayanan, D.D. Macdonald, and D.J. Wesolowski. Interfacial electrochemistry and chemistry in high temperature media. Electrochemical Society, 2008.

[65] F. Scholz. *Electroanalytical methods: guide to experiments and applications*. Springer Science & Business Media, 2009.

[66] B. Sivasankar. *Engineering chemistry*. Tata McGraw-Hill New Delhi, 2008.

[67] D. Hecht, P. Borthen, and H.H. Strehblow. An X-ray absorption fine structure study of the initial stages of the anodic oxidation of silver. *Surface science*, 365(2):263–277, 1996.

[68] J. Kunze, H.H. Strehblow, and G. Staikov. In situ STM study of the initial stages of electrochemical oxide formation at the Ag (111)/0.1 M NaOH (aq) interface. *Electrochemistry communications*, 6(2):132–137, 2004.

[69] P.S. Heljo. High frequency characterization of printed organic diodes. diploma thesis, Tampereen teknillinen yliopisto-Tampere University of Technology, 2010.